Journal of
Materials Chemistry C

Materials for optical, magnetic and electronic devices

Accepted Manuscript

This article can be cited before page numbers have been issued, to do this please use: S. H. Cho, S. Choi, J. M. Suh and H. W. Jang, *J. Mater. Chem. C*, 2025, DOI: 10.1039/D4TC04890C.

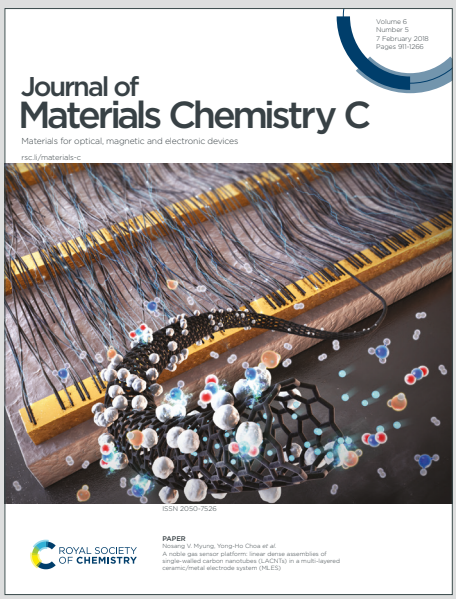

ROYAL SOCIETY OF CHEMISTRY

rsc.li/materials-c

REVIEW

View Article Online
DOI: 10.1039/D4TC04890C

Advancements in Surface Plasmon Resonance Sensors for Real-Time Detection of Chemical Analytes: Sensing Materials and Applications

Received 00th January 20xx,
Accepted 00th January 20xx

DOI: 10.1039/x0xx00000x

Sung Hwan Cho[a,‡], Seungwon Choi[a,‡], Jun Min Suh[a,‡], Ho Won Jang[a,b*]

Chemicals are being used in various fields with the development of industry, but the importance of human safety from chemicals is emerging. Instead of the traditional detection methods of analyzing analytes through preprocessing have limits in real-time circumstances On the other hands, LSPR and SPR sensors that rapidly and accurately detect chemicals in real time are one of the most reliable ways to protect against threats of chemicals. LSPR and SPR sensors are a technology that detects minute interactions between sensing materials and chemicals through changes in absorbance and refractive index, and can accurately detect even the smallest changes. In order to maximize the performance of LSPR and SPR sensors capable of real-time detection and apply them to various fields, research has been actively conducted on various types of sensing materials by ongoing research on innovative materials, fabrication techniques, and nanostructure. The future perspectives on sensing materials for real-time detection technologies used by LSPR and SPR sensors are discussed. This review presents guidelines for selecting sensing materials used in LSPR and SPR sensors in real-time applications.

1. Introduction

In modern society, the importance and versatility of chemicals in various industry, including bio, semiconductor, and agricultural industry are growing.[1,2] Additionally, as various compounds are newly synthesized or discovered, the types of chemicals used in modern society are increasing exponentially. However, as various types of chemicals are developed, concerns about the risks associated with chemicals which can have fatal effects on the human body even in small amounts are increasing.[3] For the continued development of humanity, coexistence with various types of chemicals is essential, so appropriate measures, such as early warning of chemicals emitted due to inadequate management, accidental damage, or improper disposal of chemicals, are necessary.[4]

Developing accurate methods of detection for chemical risks is a crucial technique for guaranteeing the safe use of chemicals, and various detection technologies have been developed, including inductively coupled plasma mass spectrometry (ICP-MS),[5] gas chromatography (GC),[6] and nuclear magnetic resonance (NMR).[7] However, existing methods have the disadvantage of being expensive and lacking real-time detection capabilities to detect risks early. Real-time detection which means a continuous and immediate monitoring process that provides instantaneous results or feedback as events unfold provides fast and exact information about the presence of chemicals, even at extremely low levels, separating it from traditional methods that need time consuming laboratory analyses. The capacity to give rapid data of detection methods is critical in emergency response scenarios, industrial settings, and environmental monitoring, ensuring efficient risk management.[8–10]

Sensor technology is a very popular and promising detection method due to its advantages of excellent accessibility and ability to detect in a relatively short period of time.[11,12] Sensors detect chemicals and transmit information through various methods to serve as an alarm that alerts you to danger from chemical threats. In addition to dealing with the threat, constant monitoring of air, water, food, and daily products by sensors is required to gain a basic understanding of chemical exposures and maintain safety of human beings.

Sensor technology has been developed in various ways to detect chemicals, including chemoresistive,[13] colorimetric,[14] field-effect transistor,[15] acoustic,[16] and plasmonic.[17] In addition, sensors have made many advances and plays an important role in rapid detecting very low concentrations of analytes, as a proactive safeguard, allowing for the identification, monitoring, and mitigation of possible risks to human health, environmental sustainability, and industrial safety in our complex and chemically overflowing modern society. Among various sensor technologies, researches have been actively conducted on technologies capable of accurate and real-time detection, but localized surface plasmon resonance (LSPR) and Surface plasmon resonance (SPR) sensors are gaining a lot of attention because of their low-concentration detection, instantaneous detection, and exceptional adaptability.[18–20] The excellent sensing properties of LSPR sensors at the nanoscale allows it to detect minute amounts of target molecules at the ppb level, increasing the real-time validity of detection results for trace amounts of hazardous substances.[21] Because LSPR sensor detects chemicals through changes in absorbance, it shows a color change that can be easily confirmed even with a very small amount. Based on this easy accessibility, LSPR sensors do not require complex optical systems, making it easier to miniaturize.[22] It can be integrated with microfluidics or lab-on-a-chip to construct compact systems.[23] This enables the development of small and portable sensing devices for real-

[a] Department of Materials Science and Engineering, Research Institute of Advanced Materials, Seoul National University, Seoul, 08826 Republic of Korea.
[b] Advanced Institute of Convergence Technology, Seoul National University, Suwon 16229, Republic of Korea
*E-mail: hwjang@snu.ac.kr

View Article Online
DOI: 10.1039/D4TC04890C

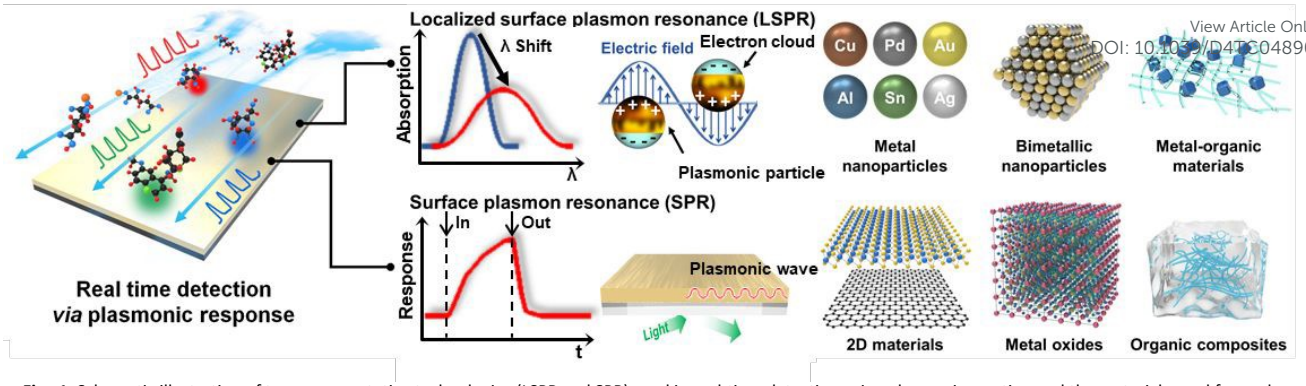

Fig. 1. Schematic illustration of two representative technologies (LSPR and SPR) used in real-time detection using plasmonic reaction and the materials used for each technology.

time and on-site detection in diagnostics, food safety, and environmental monitoring. SPR sensors, on the other hand, detect chemicals through changes in refractive index through adsorption with the sensing materials. Since these detections are based on the real-time interaction of liquid or gas as it flows, they have the advantages of being able to measure even in flowing fluids.[24] Unlike LSPR sensors, they consist of bulky optical components for accurate alignment of light, making it challenging to miniaturize them into simple devices.[22] To overcome this limitation, recent research has reported various approaches to miniaturing SPR sensors, such as reducing probe size by grating- or fiber-based SPR sensors that do not require prisms and optimizing optical design by minimizing the size of optical components.[25,26] Furthermore, SPR sensors give crucial kinetic information, allowing researchers to confirm binding events and comprehend their temporal dynamics. Both LSPR and SPR show great promise for accurate real-time detection technology, promising breakthroughs in on-site monitoring, and integration with emerging technologies, underlining their importance in the growth of analytical sciences.

The various advantages of LSRP and SPR sensors stem from the ability of the sensing materials to respond with even the slightest interaction with chemicals, and they are widely used in both biological and non-biological domains. These properties are vital as they allow for selective interactions with target analytes, ensuring that the sensor accurately and specifically responds to the desired substance. The tunability of the interactions that occur at the surface of the sensing material can improve both the specificity and sensitivity required for the detection of a wide range of chemicals, the development of which is continuously evolving. In the field of LSPR sensors, where the size and shape of nanoparticles are important, research is in progress through the shape of nanoparticles and the suitability of ligands, such as metal nanoparticles (NPs), bimetallic NPs, metal-organic materials (MOMs). On the other hand, in the field of SPR sensors, where reaction with chemicals through adsorption is important, research is being conducted on materials that can be manufactured in the form of thin films, such as two-dimensional (2D) materials, metal oxides, and organic composites, as shown in Fig. 1.

The needs for development of LSPR and SPR sensors are increasing based on their wide applicability in bio and non-bio fields, and accordingly, researches are being conducted on sensing materials suitable for each measurement method. In response to these emerging needs, active researches are being conducted in LSPR and SPR sensors, evidenced by a notable rise in the number of published papers and citations over the past decade, as shown in Fig. 2.

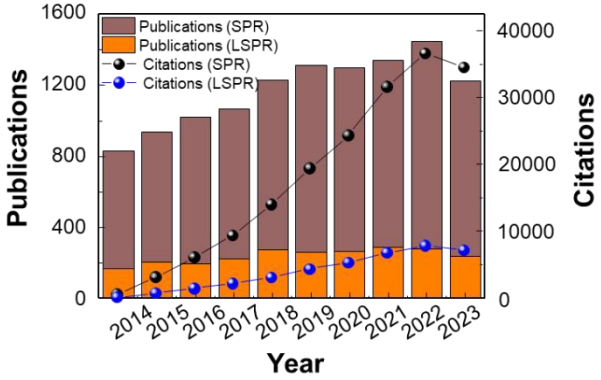

Fig. 2. Number of publications and citations on LSPR and SPR sensors. The data were collected using the Web of Science-Web of Science Core Collection Search: keywords of LSPR sensor or SPR sensor were used.

2. Principles of LSPR and SPR sensors

LSPR and SPR sensors have their roots in the broader field of plasmonics and nanotechnology. Theoretical foundations for localized plasmons were laid by theorists like Mie in 1908, with early experimental work gaining momentum in the 1980s and 1990s.[27] The development of advanced nanofabrication techniques allowed for precise control over the size and shape of NPs, influencing sensing properties. In the late 1990s, researchers recognized the potential of LSPR and SPR for sensing applications due to its sensitivity to changes in the local environment.[28,29] This led to the introduction of LSPR and SPR based sensors, enabling real-time detection at the nanoscale.

The usage of LSPR and SPR sensors has evolved significantly over the years. LSPR sensors, have found applications in diverse areas, from biomedicine to environmental monitoring.[30,31] The unique optical properties of metal NPs in LSPR allow for highly sensitive and selective detection of analytes at the nanoscale. In addition, research to improve its performance through material-based research based on metal NPs is continuing. SPR sensors, on the other hand, with their ability to monitor interactions of biomolecules and chemicals in real-time, have

View Article Online
DOI: 10.1039/D4TC04890C

become indispensable in fields such as biochemistry, pharmaceuticals, and medical diagnostics.[32] The miniaturization and integration of SPR systems, along with advancements in SPR imaging techniques, have expanded their utility to portable and point-of-care applications. Ongoing research in both LSPR and SPR continues to explore new materials, configurations, and applications, promising further advancements in the field of optical sensing technologies.

Surface plasmon is the collective oscillation of the free electrons on the surface of metals, such as gold, silver, and copper. The electric field generated by surface plasmon at the metal-dielectric interface is called surface plasmon polariton (SPP), propagating along the interface and exponentially decaying away from the surface. When a size of metal particle is comparable to the wavelength of light, the confined surface plasmon is referred to as a localized surface plasmon (LSP). An absorption peak appears at the plasmon frequency of LSP (ω_{sp}) when irradiated in the range of visible and infrared.[33]

$$\omega_{sp} = \sqrt{\frac{ne^2}{\varepsilon_0 m^*}} / \sqrt{1+\varepsilon_d}$$

where n is the electron density, e is the charge of an electron, ε_0 is the permittivity of free space, m* is the effective mass of the electron, and ε_d is the dielectric constant of the dielectrics.

The position of this absorption peak depends on the size and shape of the metal NPs, as well as the refractive index near its surface. When integrated into sensors, LSPR sensors operate by observing changes in absorption wavelength caused by interaction between the analytes and the surface of NPs. This enhanced sensitivity to minute changes in the NPs facilitates precise and real-time detection, positioning LSPR sensors as indispensable instruments in fields such as biotechnology, environmental monitoring, and medical diagnostics. A critical component in maximizing the sensing properties of LSPR based sensors lies in material research, where investigations into metal NPs strive to tailor their size and shape for enhanced sensitivity and plasmonic effects. Bimetallic NPs offer a means of fine-tuning LSPR characteristics, ensuring improved stability and durability, while MOMs introduce functionalization, amplifying selectivity and enabling multifunctionality. This holistic approach to material research, encompassing metal NPs, bimetallic NPs, and MOMs, plays an important role in increasing the versatility and efficiency of LSPR sensors in a variety of applications ranging from biomedical diagnostics to environmental monitoring.

On the other hand, in SPR sensors, polarized light is irradiated on a nanometer-thick metal thin film at a specific incident angle and wavelength. The generated SPP on metal film has the propagation constant (k_{sp}) as follows:

$$k_{sp} = \sqrt{\frac{\omega}{c}\frac{\varepsilon_m \varepsilon_d}{\varepsilon_m + \varepsilon_d}}$$

where ε_m and ε_d are the dielectric constants of metal and dielectrics, ω is the frequency of incident light, and c is the velocity of light.

When the propagation constant of SPP and the wavevector of incident polarized light matches well, SPR occurs on the surface of metal film.[34] The resonance angle and wavelength are sensitively influenced by changes in the refractive index near the metal surface. The adsorption of analytes induces a fluctuation of the refractive index near the metal surface and influences the resonance angle and wavelength. Through tracking resonance conditions, the interaction and kinetics between analytes and sensing materials can be monitored sensitively in real-time. Their importance lies in applications such as drug discovery, medical diagnostics and environmental monitoring due to their exceptional sensitivity and binding kinetics of sensing materials. Concurrently, research focused on the recognition layer which is a thin functionalized sensing material on the sensor surface, responsible for adsorbing chemicals in SPR sensors, proves indispensable for optimizing sensor performance. Sensing materials in this recognition layer are being researched for their potential application in 2D materials such as graphene, which offer improved biocompatibility and high surface-to-volume ratio for enhanced sensitivity and real-time detection. Metal oxides improve sensitivity and find value in applications such as environmental monitoring through their low cost and easy and versatile synthesis methods. Additionally, organic composites with customized functionalization are highly suitable for biomedical and chemical sensing due to their high selectivity, enabling detection of the desired chemical. The ongoing investigation and refinement of material choices for the recognition layer constitute pivotal strides in advancing SPR sensors for a spectrum of applications, spanning from medical diagnostics to environmental analysis.

3. Real-time monitoring properties of LSPR sensors

LSPR sensors offer distinct advantages for chemical real-time detection over other technologies in terms of versatility and accuracy. The real-time monitoring capabilities of LSPR sensors allow continuous observation of chemicals to gain insight into the kinetics, and affinity of interaction between sensing materials and chemicals. The low detection limit and great sensitivity of the LSPR sensor are due to the characteristics of the sensing material, which changes its shape and size even with the slightest change, and with the development of optical measurement equipment, even minute changes in absorbance can be accurately measured. Additionally, LSPR sensor has the advantage of being able to detect chemicals with the naked eye without measuring equipment by detecting chemicals through changes in absorbance even with a small amount of sensing material. These various advantages improve the portability and applicability of LSPR sensors, allowing efficient, low-cost detection without restrictions in various fields where chemicals exist. Overall, the comprehensive attributes of LSPR sensors

View Article Online
DOI: 10.1039/D4TC04890C

make them powerful tools for diverse applications in chemical sensing. The adaptability and versatility of LSPR sensors extend their utility across a wide range of applications, including biochemistry, environmental monitoring, medical diagnostics, and food safety. The wide applicability and ability to provide real-time information contribute to its widespread adoption in both research and industrial settings.

The advantages of LSPR sensors position them as valuable tools in the field of sensing technologies, offering unique capabilities for precise, efficient, and real-time detection in chemical applications. Thus, diverse sensing materials are required to improve the sensing performance and real-time detection ability. Research is being actively conducted on metal NPs that most easily exhibit the LSRP phenomenon,[35–44] LSPR sensors with improved characteristics using various bimetallic NPs,[45–54] and material-based LSPR sensors that improve sensitivity by using organic particles in metal nanoparticles are summarized in the Table 1.[55–60]

Table 1. Summary of LSPR sensors based on metal NPs, bimetallic NPs, and MOMs.

Material type	Target type	Sensing materialsa)	Analyte	Detection range	Limit of Detection	Ref.
Metal NPs	Bio	AuNRs	β-galactosidase	0.1-10 nM	128 pM	[35]
		AgNPs	Melamine	0-10 μM	0.099 μM	[36]
		AgNPs	Timolol	0.1-1000 μM	1.2 μM	[37]
		AgNPs	Aflatoxin B1	1-10 ng/ml	0.36 ng/ml	[38]
		AgNPs	Cholic acid	0-30 μM	1 μM	[39]
		AgNPs	Omeprazole	0.05-40 μM	15 nM	[40]
	Non-bio	AuNRs	Cu^{2+}	0-1 mM	0.5 nM	[41]
		AgNPs	Cd^{2+}	1-10 μM	87 nM	[42]
		AgNPs	As^{3+}	5-500 μg/L	2 μg/L	[43]
		Ag NPR	Hg^{2+}	0.005-10 μM	0.2 nM	[44]
Bimetallic NPs	Bio	Ag/Au nanoshell	Glucose	0.002-2 mM		[45]
		Au nanocage	Gallic acid	0.01-5 μM		[46]
		Au nanocage	Vitamin C	0.05-7.5 μM	0.024 μM	[47]
		AuNRs	Ellagic acid	0.2-20 μM	0.04 μM	[48]
	Non-bio	GSH-s-Au/Ag nanoframe	Co^{2+}	1.7-17 μM	0.04 μM	[49]
		Pd/Au/Cu	H_2			[50]
		Au nanosphere/ AgNRs	ClO^-	0.5-30 μM	0.24 μM	[51]
		Au/Ag nanocage	Hg^{2+}	0.03-35 μM	10 nM	[52]
		Au/Ag/AgCl core-shell NPs	NH_3	0-5000 μM	6.4 μM	[53]
		Ag/Cu NPs	Hg^{2+}	0.001-50 μM	0.51 nM	[54]
MOMs	Bio	Ag NPR / Glucose oxidase	Glucose	0.2-100 μM	0.2 μM	[55]
		Sucrose capped AuNPs	Daclatasvir	0.01-1 μg/ml	0.008 μg/ml	[56]
		Amine/POSS-APBAs/AuNPs	Glucose	1-1000 μM	25 μM	[57]

View Article Online
DOI: 10.1039/D4TC04890C

Non-bio	SA-AgNPs/PVA nanocomposites	Hg^{2+}	0.9-1200 ppb	0.9 ppb	[58]
	AuNPs/PO-EGMA	Pb2+	0.1-100 nM	25 pM	[59]
	Melamine-Au nanostars	Uric acid	0-100 µM	8.5 nM	[60]

3.1 Metal NPs based LSPR sensor

Metal NPs based LSPR sensors are now widely used in sensing technology. The high surface-to-volume ratio and adjustable properties of these NPs, regulated by their form, make them ideal for immobilizing target molecules.[61,62] The exact geometry of metal NPs has a substantial impact on their plasmonic resonance frequencies, allowing for fine tuning to meet the desired wavelength. Metal NPs exhibit a unique characteristic where their light absorption wavelength changes based on variations in shape and size due to minuscule interactions with chemicals. This property enhances sensitivity to environmental changes of LSPR sensors, resulting in superior detection capability and precision. The adaptability of structuring metal NPs allows for subtle control over localized electromagnetic fields, which affects the detection capabilities of LSPR sensors. With these considerations, LSPR sensors based on metal NPs, with their shape dependent effects, have found significant use in biomedical diagnostics, environmental monitoring, and chemical sensing. This highlights their ability to provide high-performance and adaptable sensing technologies that meet the specific needs of various areas.

3.1.1 Biosensors applications

Among LSPR sensors that detect through metal NPs of various shapes, Chen et al. reported research on detecting β-galactosidase (β-gal) using Au nanorods (NRs).[35] Real-time detection technology for β-gal is indispensable for uncovering the dynamics of gene expression, understanding cellular processes, capturing dynamic cell behaviors, and optimizing various biotechnological and medical applications. The real-time aspect enables a more nuanced and comprehensive analysis, providing researchers and practitioners with valuable insights into the temporal aspects of β-gal-mediated processes across different scientific domains.

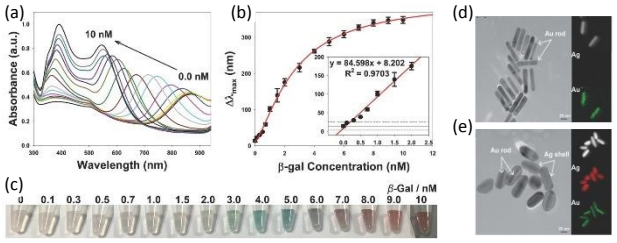

Fig. 3. (a) UV-vis absorption spectra and (b) the blue shift in the longitudinal LSPR peak of Au NRs to β-gal (0 to 10 nM). (c) Photographs of multicolorimetric assays of AuNRs toward various concentrations of β-gal. TEM images of AuNRs (d) before and (e) after incubation of β-gal. Reproduced with permission from ref. 35 Copyright © 2016 John Wiley & Sons.

The sensing mechanism described involves a multicolorimetric assay using AuNRs and enzyme-induced metallization. In the absence of β-gal, the unhydrolyzed substrate, p-aminophenyl β-D-galactopyranoside (PAPG), cannot reduce Ag^+ to metallic Ag. As a result, the solution retains the initial color of the AuNRs, appearing light pink. However, in the presence of β-galactosidase, it cleaves PAPG into galactoside and a reducing agent (PAP). This reducing agent, in the presence of AuNRs, then reduces Ag^+ to metallic Ag. The reduced metallic Ag coats the surface of AuNRs, inducing a multicolor shift in the sample solution. Consequently, the color of the solution transitions from light green to orange-red, correlating with the concentration of β-gal. This multicolorimetric assay provides a visual indication of β-gal presence, allowing for a qualitative and potentially quantitative assessment based on the observed color changes in real-time.

The researchers used the absorbance spectra to monitor the change of AuNRs in varying β-gal concentrations (Fig. 3a). As the concentration increases, the absorbance of the AuNRs increases and the wavelength absorbed decreases. A dynamic relationship between $\Delta\lambda_{max}$ and β-gal concentration was seen within the range of 0.1×10^{-9} to 10×10^{-9} M, as shown in Fig. 3b. Fig. 3b demonstrates that the $\Delta\lambda_{max}$ value increased as the concentration of β-gal. As the concentration increases, the amount of change in the wavelength decreases, but at low concentrations, the correlation between concentrations and $\Delta\lambda_{max}$ can be seen to be linear. This change in $\Delta\lambda_{max}$ can also be observed as a color change in the solution. As shown in Fig. 3c, the detection solutions exhibited a color shift from light green to orange-red as compared to the control. The distinct multicolor changes at the concentration of 2.0×10^{-9} M can be easily identified visually. In Fig. 3d and e, the transmission electron microscopy (TEM) image shows the synthesized AuNRs with a length of 59 ± 8 nm and a width of 11 ± 1 nm. After the reaction the Ag shell on the body sides of AuNRs was observed. The deposition of Ag shell on the surface of AuNRs was further investigated using High-resolution TEM-energy dispersive X-ray spectroscopy (EDS). The corresponding EDS Ag (red color) and Au (green color) mapping images also confirmed the coating of metallic silver on the surface of AuNRs. The Ag peaks in the EDS spectrum were observed after the enzyme induced metallization. Both enhanced absorbance intensity and blue shift of the longitudinal LSPR peak were observed after enzyme induced Ag metallization on the surface of AuNRs. The longitudinal LSPR peak shifted from 885 to 520 nm, and the

absorbance intensity of longitudinal LSPR peak likewise increased with the increasing of β-gal concentrations.

3.1.2 Non-biosensors applications

The increase in heavy metal exposure poses a major risk to human health. Heavy metals including Pd, Hg, Cd and As are well-known for their toxic effects on the brain system, kidneys, and other organs.[63,64] Prolonged exposure to high levels of these metals is linked to an increased risk of neurological issues, developmental abnormalities, renal damage, and some malignancies. The hazard is worsened by heavy metal bioaccumulation in the food chain, which allows toxic elements to be absorbed by plants and aquatic species before reaching human populations via polluted food and water. Thus, the current increase in the prevalence of heavy metal ions poses a major and far reaching threat to human well-being, needing immediate action to monitor, regulate, and minimize their influence on both human health and the environment. Many analysis methods have been developed to detect ions that have a very negative effect on the human body. While these approaches provide high sensitivity and multi-element analysis, they are costly, time consuming, complex, and challenging for on-site field testing. LSPR sensors, however, possess not just the advantages of current detection technologies, but also provide instantaneous detection. Their multiplexing property enables the simultaneous detection of numerous heavy metal ions, improving analytical efficiency. The ability to design the characteristics of metal NPs in LSPR sensors allows for customizing to specific heavy metal ions and sample circumstances. With minimal sample preparation requirements, portability, and the potential for cost-effective analysis, LSPR sensors are well suited for on-site monitoring in a variety of settings, from environmental monitoring to industrial applications, making them a valuable tool for addressing the critical challenges associated with heavy metal ion contamination.

Chen et al. reported LSPR Hg^{2+} sensor based on the shape change of unmodified Ag nanoprism (AgNPR) by adding Hg^{2+} and $S_2O_3^{2-}$.[44] The proposed sensing mechanism in this study involves apical activation and passivation of triangular AgNPR through the actions of $S_2O_3^{2-}$ and Hg^{2+}. $S_2O_3^{2-}$ acts as a leaching agent, rapidly truncating the sharp tips of unmodified AgNPR into round nanodiscs, resulting in a distinct color change and a significant shift in the LSPR wavelength. This change is prevented in the presence of Hg^{2+}, which protects the AgNPR from etching by forming HgS at the corner sites. The AgNPR shape is thus frozen, allowing for the quantization of Hg^{2+} ions in the solution, as shown in Fig. 4a. The optical properties of the prepared AgNPR colloid, including a blue color and distinct LSPR absorption bands, are highly sensitive to trace reactions, controlling the edge length, thickness, and sharp tips of the AgNPRs. The sculpturing effect of $S_2O_3^{2-}$ and passivation effect of Hg^{2+} are illustrated through changes in colloidal color and absorption spectra, as shown in Fig. 4b. The addition of $S_2O_3^{2-}$ induces facet selective etching reactions, leading to a blue to yellow color change and a blue-shift in the LSPR peak. In the

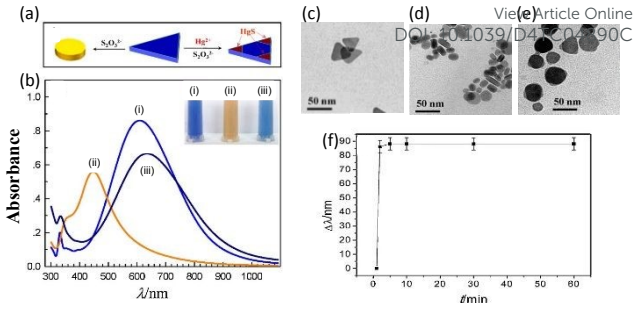

Fig. 4. (a) Schematic illustration of shape evolution of a AgNPR and growth of HgS in the presence of $S_2O_3^{2-}$ and Hg^{2+}. (b) UV–vis spectra and photographs (inset) of AgNPR with 3 different conditions ((i) as-prepared, (ii) with $S_2O_3^{2-}$, and (iii) with $S_2O_3^{2-}$ and Hg^{2+}). TEM images of AgNPR: (c) as-prepared and with the addition of (d) $Na_2S_2O_3$ and (e) Hg^{2+} and $Na_2S_2O_3$. (f) Wavelength shift as a function of the reaction time of the AgNPR–Hg^{2+}–$Na_2S_2O_3$ mixture, pH 2.9. Reproduced with permission from ref. 44 Copyright © 2015 Elsevier B. V.

presence of both $S_2O_3^{2-}$ and Hg^{2+}, the color change and LSPR shift are halted due to the formation of insoluble HgS at the tips of AgNPR. The changes in the shape of individual AgNPRs in three separate cases can also be verified using TEM analysis. TEM imaging revealed the original triangular shapes of AgNPR (Fig. 4c), circular nanodisc shapes in the presence of $S_2O_3^{-}$ (Fig. 4d), and additional angles in the presence of both $S_2O_3^{-}$ and Hg^{2+} (Fig. 4e).

Fig. 4f demonstrates that the reaction can reach a steady state within 5 minutes, allowing for quick detection and real-time detection. The concentration of Hg^{2+} can further tune the color change and LSPR wavelength, providing distinctive characteristics for wide range Hg^{2+} detection within a short timeframe. The dominant interaction among AgNPR, $S_2O_3^{2-}$, and Hg^{2+} is identified as HgS deposition reactions within 5 minutes, contrasting with the longer etching reactions observed without $S_2O_3^{2-}$.

Metal NPs based LSPR sensors with color shift due to agglomeration are a dynamic and responsive sensing platform. Metal NPs, often Au or Ag, are scattered in a solution to form these sensors. When exposed to specific analytes, the NPs aggregate, changing their spatial arrangement and causing a shift in the plasmonic resonance. This agglomeration induced alteration appears as a distinct color shift in the solution, providing a visible readout. The color change mechanism provides an immediate and understandable indication of the presence and concentration of target analytes, making these sensors ideal for applications requiring a quick and qualitative response. The issue of regulating agglomeration in these systems emphasizes the significance of careful design and optimization to improve the reliability and sensitivity of color changing LSPR sensors in a variety of analytical and detecting applications.

3.2 Bimetallic NPs based LSPR sensors

Bimetallic NPs exhibit synergistic effects, where the interplay between the two metals influences the resonant frequency, and nanostructure, resulting in enhanced sensor performance. In addition to improved stability and durability, the distinctive

View Article Online
DOI: 10.1039/D4TC04890C

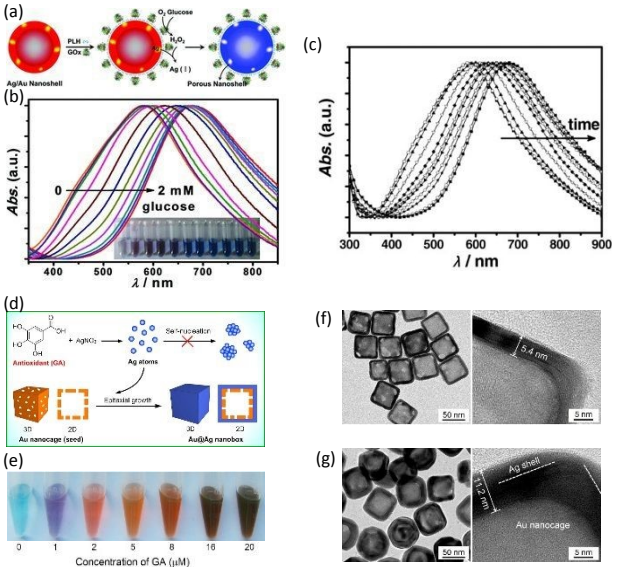

Fig. 5. (a) The fabrication process of Ag/Au bimetallic NSs and sensing mechanism. (b) The normalized UV-vis extinction spectra of Ag/Au NSs after incubation with glucose in various concentrations (0 to 2 mM) (c) Time-dependent UV-vis absorption spectra of Ag/Au bimetallic NSs upon incubating with 3 x 10^{-3} M glucose. Reproduced with permission from ref. 45 Copyright © 2012 John Wiley & Sons. (d) Schematic illustration of Au/Ag nanobox fabrication. (e) color changes for the creation of Au/Ag nanobox at various concentrations of gallic acid. TEM images of (f) Au nanocages for absence of gallic acid and (g) Ag/Au nanoboxes for presence of gallic acid. Reproduced with permission from ref. 46 Copyright © 2018 Elsevier B. V.

characteristics of bimetallic materials, such as more flexible morphological tunability, enable visual detection through multicolor changes and enhance sensitivity and accuracy in LSPR sensing applications across diverse fields, including biomedical diagnostics, environmental monitoring, and chemical analysis.

3.2.1 Biosensors applications

He et al. exhibited Ag/Au bimetallic nanospheres (NSs) utilized glucose oxidase (GOx) system to detect glucose by LSPR tehcnology.[45] The hollow and intact Ag/Au bimetallic NSs used as sensing platforms were synthesized using a colloid seed engaged replacement reaction and a colloid mediated deposition reaction, with hydroxylamine hydrochloride as a mild reducing agent. The Ag/Au-GOx NSs complex was then generated via electrostatic adsorption of the negatively charged GOx protein (PI = 4.2) onto the positively charged polyhistidine coated NS surface at pH 6-7. During the procedure, an excess quantity of GOx was employed to achieve monolayer saturation on the NSs surface. As shown in Fig. 5a, He's group reported LSPR sensor based on the selective dissolution of Ag from the produced hollow Ag/Au bimetallic NSs by hydrogen peroxide, which is derived from the surface confirmed enzymatic oxidation of glucose in the presence of oxygen. As the enzymatic H_2O_2 etching progresses, the surface plasmon band of the resulting porous NSs gradually redshifts, reflecting the concentration change of hydrogen peroxide, which in turn is a measure of the concentration change of glucose in the reaction system. The sensitivity of the sensor was believed to be increased by confining GOx onto the Ag/Au NSs surface by electrostatic adsorption.

They investigated the sensitivity and applicability of the Ag/Au-GOx NSs system for optical glucose sensing. In this measurement, 1 mL aliquots of the as-prepared Ag/Au-GOx NSs suspension were incubated with 20 µL glucose solutions with a final concentration ranging from 0.002 x 10^{-3} to 2 × 10^{-3} M for 30 minutes. Fig. 5b shows a steady red-shift of the LSPR peak and a clear color change as the glucose concentration increases. A linear association was found between the LSPR peak shift of $\Delta\lambda_{max}$ and glucose concentration, ranging from approximately 0.5 × 10^{-6} M to 0.02 × 10^{-3} M.

Evaluating the real-time detection capability of a sensor can be effectively done by observing changes over a period of time. Fig. 5c displays the UV-vis spectra of the nanocomplex over time when incubated with a glucose concentration of 3 × 10^{-3} M. The λ_{max} of nanocomplex progressively moves to longer wavelengths when glucose was injected. After around 1-2 hours, the shift levels off and reaches a saturation value. An observable transition in color, shifting from red-violet to blue, occurred within a time frame of ten minutes. This implies that the Ag/Au-GOx NSs have the potential to be utilized for practical colorimetric detection of glucose.

Nanostructures, with their small size and high surface-to-volume ratio, improve sensing properties in a variety of applications.[13] The increased surface area of nanostructured materials creates more active sites, resulting in more significant interactions with target analytes. The morphological change of Au nanocage to Au@Ag nanobox, and thus the LSPR evolution, are efficiently regulated by trace amounts of antioxidant, which act as both a reductant in seed-mediated growth and a detecting target. Ag atoms can be produced through a redox reaction between Ag^+ and an antioxidant, such as gallic acid, as utilized in this study.[46] When Au nanocages (seeds) with a cubic shape, hollow interior, and numerous holes in the wall are present, newly generated Ag atoms deposit uniformly on the seeds' surface by heterogeneous nucleation rather than self-nucleation. This results in the creation of Au@Ag nanoboxes with a hollow interior and closed wall (Fig. 5d). A new colorimetric approach for antioxidant assessment is devised using the morphological changes of nanoprobes and triggered LSPR evolution in the absence and presence of antioxidants.

This technique achieves high sensitivity by heterogeneous nucleation of metal NPs, which requires a lower energy barrier compared to self-nucleation. Fig. 5e shows sample photographs of the color change of solution at various gallic acid doses (0 to 20 µM). As Gallic acid content increased, the color changed from dark green to blue, red, orange, and brown.

The TEM images in Fig. 5f reveal hollow cubic Au nanocages with an outside edge length of 54.2 ± 3.5 nm and a wall thickness of 5.4 ± 0.8 nm. The pores on the side faces of the Au nanocages confirm the characteristic nanocage morphology. In the presence of 4 µM gallic acid, cubic nanocages converted into nanoboxes with hollow inners and closed walls. Compared to the original nanocages, the nanoboxes had significantly longer outer edges and thicker walls (Fig. 5g). The nanoboxes had an average size of 65.8 ± 5.3 nm, indicating an Ag layer of

approximately 5.8 nm on the surface of Au nanocages. TEM images at higher magnification reveal the outer layer of Ag and the contained nanocage due to the contrast between Au and Ag.

3.2.2 Non-biosensors applications

The primary focus of research on sensors utilizing plasmons has been on solution based analytical technology that relies on intense interaction with the analyte. Additionally, gas detection technology requires selective detection of various unknown substances and stability to maintain detection characteristics even in extreme environments because of poisoning effect.[65] Nevertheless, there is still a significant amount of research being done and a need for technology that can detect low concentration of gases at room temperature selectively.[66] Among various sensing materials, Pd is being investigated as a material for LSPR sensors due to its dual properties of significant catalytic activity for hydrogen and plasmon resonance effect.[67]

Darmadi et al. recently demonstrated that a ternary PdAuCu alloy for plasmonic optical hydrogen detection could provide a solution to the poisoning effect.[50] They initially explored ternary PdAuCu nanoparticle arrays created using hole-mask colloidal lithography, which consisted of quasi-random configurations of nanodisks with an average diameter of 190 nm and a height of 25 nm (Fig. 6a). Au primarily contributes to the closure of the hysteresis gap, whereas Cu causes an elevation of the plateau region to higher hydrogen partial pressures. In the context of hydrogen sensors, the optimal ternary alloy composition is a balance between eliminating the hysteresis gap and maximizing the magnitude of $\Delta\lambda_{max}$ per hydrogen partial pressure change. Criterion (i) requires alloys with at least 25% Au, whereas criterion (ii) limits Au and Cu concentrations as increasing them reduces total sensor sensitivity due to reduced peak per hydrogen partial pressure change. As a result of these selection

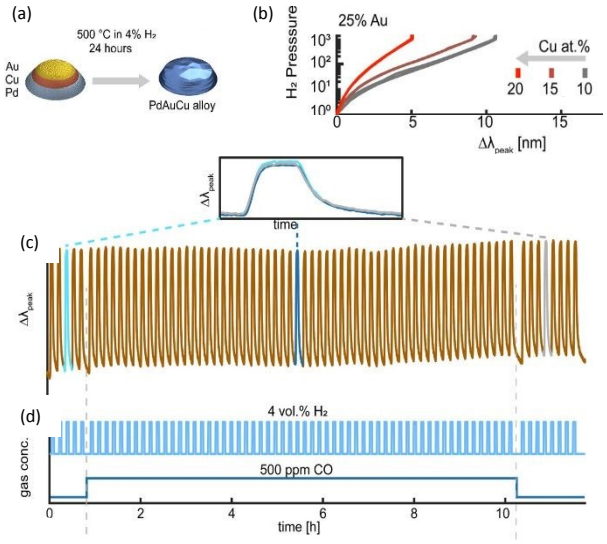

Fig. 6. (a) Schematic illustration of PdAuCu alloy NPs fabrication. (b) Pressure-$\Delta\lambda_{peak}$ for PdAuCu ternary alloys with 25% Au concentration of 10, 15, 20% Cu content. (c) Temporal response of $\Delta\lambda_{peak}$ for $Pd_{65}Au_{35}Cu_{10}$ alloy system to 4 vol. % H_2 pulses in synthetic air at 30°C, (d) with and without the 500 ppm CO background. Reproduced with permission from ref. 50 Copyright © 2021 American Chemical Society.

criteria, the $Pd_{65}Au_{25}Cu_{10}$ ternary alloy system is identified as the best compromise and hence our champion system. It is worth noting that the tiny gap between the absorption and desorption branches seen in Fig. 6b for the $Pd_{65}Au_{25}Cu_{10}$ alloy is a measurement artifact rather than an intrinsic hydride hysteresis gap. The absence of the α−β phase transition along the curve suggests hysteresis-free hydride production.

Darmadi's group investigated the resistance of $Pd_{65}Au_{25}Cu_{10}$ to poisoning, as shown in Fig. 6c. They exposed it to over 50 pulses of 4% H_2 for 5 minutes each, while maintaining a steady background of 500 ppm CO which is sidely known to interfere with reaction with hydrogen, in synthetic air carrier gas at a temperature of 30°C.[68] The experiment lasted for 12 hours, as shown in Fig. 6d. The LSPR sensor exhibited remarkable stability and resistance to deactivation, as evidenced by its consistent response and recovery times throughout the whole experiment. The overall morphology and configuration of the nanodiscs on the surface, however, remain unaltered even after the extended duration of the test.

Bimetallic NPs based LSPR sensors are a sophisticated type of sensing platform that takes advantage of the synergistic features of two distinct metals, typically Au and Ag or Au and Cu. The metal combination allows for more tuning and control over the plasmonic sensing properties. Bimetallic NPs have distinct optical characteristics, which provide additional information for sensing applications. The different electrical and catalytic properties of each metal in the bimetallic framework help to improve sensitivity and selectivity when detecting target analytes. These sensors find applications in a variety of sectors, including environmental monitoring and biomedical diagnostics, where their customized composition enables fine tuning to specific detection requirements. The use of bimetallic NPs into LSPR sensors demonstrates a diverse and advanced strategy that improves the capabilities of plasmonic sensing technologies for precise and reliable detection.

3.3 MOMs based LSPR sensors

MOMs have garnered attention for their unique properties in the context of LSPR sensors. MOMs are hybrid materials comprised of metal nodes interconnected by organic ligands, offering a diverse and tunable platform for LSPR applications. By incorporating various ligands into these structures, researchers can precisely control the properties of the resulting MOMs, influencing their electronic and optical characteristics. The surface functionalization of metal NPs provides selectively binding sites and prevents the dissociations of metal NPs, leading to reversible measurements. This versatility allows for tailoring the LSPR response to specific applications, enhancing the sensor's sensitivity and selectivity. The integration of MOMs in LSPR sensors with various ligands opens up possibilities for a wide range of functionalities, making them promising candidates for advanced sensing technologies in fields such as chemical analysis, environmental monitoring, and biomedical diagnostics.

3.3.1 Biosensors applications

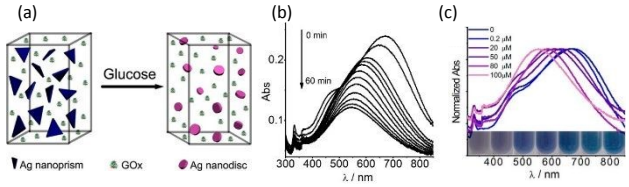

Fig. 7. (a) Schematic illustration of Ag-GOx composite for glucose sensing. (b) Time-dependent LSRP absorption spectra of the Ag NPR upon incubating with 100 μM of glucose (0 to 60 min). (c) Normalized LSRP absorption spectra of Ag-GOx to various concentrations of glucose (0 to 100 μM). Reproduced with permission from ref. 55 Copyright © 2013 American Chemical Society.

Xia et al. presents a simple but successful technique for colorimetric imaging of glucose at the submicromole level in blood utilizing unaltered Ag nanoprisms, with little theoretical complexity and physical requirements.[55] The sensing steps are shown in Fig. 7a. First, GOx and Ag nanoprisms were simply combined and glucose was then added to the homogenous mixture ultimately, Ag triangle nanoprisms were etched to round nanodiscs by H_2O_2 created by enzymatic oxidation. The detection limit was 0.2 μM, lower than that of previously reported hybrid metal NP-GOx systems. The exceptional sensitivity was attributed to (1) extremely reactive edges/tips and (2) substantially tip sharpness and aspect ratio dependent LSPR absorption of Ag nanoprisms.

The time-dependent LSPR band of the homogeneous system that was exposed to a concentration of 0.1 mM glucose during incubation are shown in Fig. 7b. The in-plane dipole band shift is observed to rapidly diminish within the first 10 minutes (90 nm), followed by a gradual decline until it reaches a saturation value after around 30 minutes. Photograph of LSPR sensor shows a steady blue shift of the in-plane dipole band and a clear color change of the Ag nanoplates (blue to purple to mauve) with increasing glucose content, as shown in Fig. 7c. This change in color is due to a change in the shape of Ag through reaction. Due to its excellent sensitivity, only 10-20 μL of serum is sufficient for a single measurement. The proposed sensing device was extremely convenient: the entire process, from Ag nanoprism creation to test completion, took less than an hour.

3.3.2 Non-biosensors applications

Subu et al. reported another MOMs based poly vinyl alcohol (SA-Ag/PVA) nanocomposite thin films which can detect Hg^{2+} which is one of the most fatal heavy metal ion to human beings.[58] Na-alginate reduced SA-Ag/PVA nanocomposite thin films were created by a simple synthetic technique. Rather than employing a functional monomer or cross-linking agent, they used sodium alginate, a biopolymer, for the imprinting process. The compound's functional groups, including COOH, OH, and NH_2, allow it to combine with Ag^+ (aq). After thermal activation, the OH functionality works as a bio-reducing agent, converting Ag^+ to Ag. The resulting AgNPs are stabilized inside the sodium alginate network by various functional groups. The AgNPs-imprinted sodium alginate network was converted into a nanocomposite thin film using polyvinyl alcohol (PVA), as shown in Fig. 8a.

The functional groups containing oxygen in PVA have a binding affinity for Hg and Hg2+, allowing them to diffuse into the nanocomposite film. Because the reduction potential of Hg2+/Hg is higher than that of Ag+/Ag, Ag is oxidized to Ag^+ and Hg2+ is reduced to Hg, forming Ag/Hg amalgam and depositing Hg within SA-Ag/PVA film simultaneously. This influences the position and intensity of the LSPR peak for AgNPs within a few minutes. Fig. 8b exhibits the UV-vis spectra of SA-Ag/PVA nanocomposite thin films for 10 minutes in aqueous solution with 1000 ppb of Hg^{2+} ions. Even after 2 minutes, the inclusion of Hg2+ causes a blue shift of LSPR peak and decreases the intensity rapidly. The researchers also detected Hg2+ concentrations ranging from 2 to 1200 ppb and showed the good linearity of absorption intensity, where correlation coefficient was larger than 0.99. Furthermore, the sensor can detect Hg^{2+} concentrations ranging from 2 to 1200 ppb. The sensor SA-Ag/PVA nanocomposite thin film has computed LOD and LOQ values of 0.9 ppb and 3.07 ppb for Hg^{2+}, respectively.

The AuNPs-poly(oligo-(ethylene glycol)methacrylat) (POEGMA) system was used to detect lead, which is classified as a major environmental pollutant due to its high toxicity.[59] Fig. 8c depicts the resultant sensing platform, which was developed using a detection chemical based on AuNP leaching. First, AuNPs immobilized in POEGMA are functionalized with thiosulfate (by thiosulfate adsorption on AuNPs surface). Thiosulfate-functionalized AuNPs dissolve in the presence of 2-mercaptoethanol (2ME) and Pb^{2+} ions, forming Au–Pb alloy on the AuNP surface and soluble Au^+–2ME complexes. Leached AuNPs with Au-Pb alloy on their surface no longer interact strongly with the brush's EG chains, allowing them to be released into solution. AuNP release from the POEGMA matrix reduces UV-vis absorbance and color fading in the AuNP-POEGMA coated glass cover slip. This detection technique was chosen primarily because similar chemistry has been shown to detect lead with good sensitivity and specificity in solution. As a

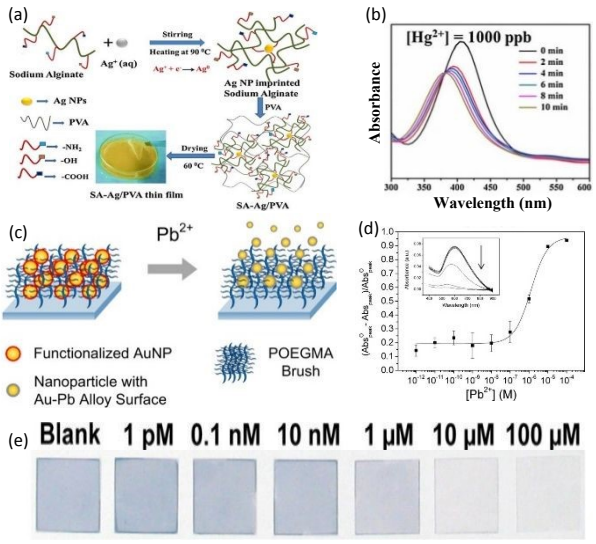

Fig. 8. (a) Schematic illustration of SA-Ag composite thin film for Hg^{2+} sensing. (b) The LSPR peak of SA-Ag composite in aqueous solution of 1000 ppb of Hg^{2+}. Reproduced with permission from ref. 58 Copyright © 2017 Elsevier B. V. (c) Pb^{2+} sensing mechanism of functionalized AuNPs. (d) Responses and (e) photograph with to various concentrations of Pb^{2+} ranging from 1 pM to 100 μM. Reproduced with permission from ref. 59 Copyright © 2013 American Chemical Society.

View Article Online DOI: 10.1039/D4TC04896C

result, the performance in solution would be a useful baseline for comparing our solid-phase system. Furthermore, unlike in-solution detection, which involves mixing thiosulfate and 2ME with the target and AuNPs in a single step, we were able to isolate the thiosulfate adsorption step here. This shows that preloaded AuNPs can be post-functionalized within the polymer brush using alternative detection techniques of interest. The detection capability of AuNPs in POEGMA was studied by immersing the substrates in water containing Pb^{2+} varying from 1.00 pM to 100 μM in the presence of 2ME and calculating absorbance drops, as shown in Fig. 8d. Fig. 8e show images of AuNP-POEGMA samples after Pb^{2+} detection. POEGMA-coated samples are easily identifiable with unaided eyes because to a higher AuNP loading.

4. Real-time monitoring properties of SPR sensors

SPR sensors exhibit several advantages in chemical real-time detection, distinguishing them from other detection technologies. A variety of analytes above the surface of metals are sensed through adsorption on the sensing materials, allowing detection of even minute levels in both liquid and gas. Also, SPR sensors are suitable for real-time measurement as it detects the interaction with chemicals in a fluid in motion. This simplifies experimental procedures, reduces potential interferences, and enables a direct and real-time observation of molecular binding events. SPR sensors excel in providing real-time kinetic data, offering insights into the association and dissociation rates of chemicals, which is crucial for understanding the dynamics of interactions between chemicals and sensing materials. The high sensitivity of SPR sensors allows the detection of molecular interactions at low concentrations, making them particularly valuable for applications requiring precise and quantitative analysis of chemicals.

SPR sensors have the advantage of being adaptable to a wide range of sensing materials that can selectively interact with the specific chemical being studied. SPR sensors possess high sensitivity, enabling precise monitoring of molecule interactions even at low concentrations, down to the picomolar or femtomolar level. This adaptability applies to a range of sensing materials, allowing modification based on the specific characteristics of the target chemical and enabling immediate analysis of complicated materials, such as biological fluids. Additionally, SPR sensors are suitable for studying complex chemicals, offering a real-time approach to analyze binding kinetics in a native environment. These attributes make SPR sensors as powerful tools in chemical sensing, providing

Table 2. Summary of SPR sensors based on 2D materials, metal oxides, and organic composites.

Material type	Target type	Sensing materials[a)]	Analyte	Detection range	Limit of Detection	Sensitivity	Ref.
2D materials	Bio	ADP3NSs	Amyloid-beta 1-42	1-10^4 pM	1 pM		[69]
		AuNPs/GeP_5NSs	SARS-CoV-2 RNA	10^{-2}-10^4 fM	10 aM	146 °/RIU	[70]
		SsDNA/Cu-TCPP	Dopamine	5-5x10^5 pM	0.15 pM	2820.83 nm/RIU	[71]
		MoS_2NSs	Ferritin	50-400 ng/mL	Ferritin: 12 ng/mL	Ferritin: 0.024 nm/(ng/mL)	[72]
		Ti_3C_2-MXene/AuNPs	Carcinoembryonic antigen	2x10^{-4}-2x10^4 pM	0.07 fM		[73]
		Peptide/Cu-TCPP NSs	Programmed death ligand-1 exosome	10^4-5x10^6 particles/mL	16.7 particles/mL	137.67 °/RIU	[74]
		Graphene/Au	Glucose	0-300 mg/dL		3113 nm/RIU	[75]
		AuNRs-ssDNA/SbNSs	microRNA-21	10^{-2}-10^4 fM	10 aM	171 °/RIU	[76]
	Non-bio	Graphene	2,4 Dinitrophenol	100~500 ppb	3 ppb		[77]
		Ti_2C-MXene NSs	Pb^{2+}	1-20 μg/L	79.2 ng/L	3.788 nm/(μg/L)	[78]
Metal Oxides	Bio	ZnONPs /$MoSe_2$NSs	Glucose	0-1.2 mg/mL	4.16 μg/mL	72.17 nm/(mg/mL)	[79]
		Ta_2O_5NFs	Xanthine	0-3 μM	0.0127 μM	26.204 nm/μM	[80]
		Fe_3O_4	Glucose	0.1-10 mM	19.95x10-2 mM		[81]
		ZnO nanowires/CeO_2	Dopamine	10^{-3}-10 pM		95 °/RIU	[82]

View Article Online
DOI: 10.1039/D4TC04890C

		ZnO	Neisseria meningitidis DNA	10-180 ng/μL	5 ng/μL	0.037 °/(ng/μL)	[83]
		Ta_2O_5 NPs embedded in rGO	Fenitrothion	0.25-4 μM	38.2 nM	24.02 nm/μM	[84]
	Non-bio	WO_3	NO_2	0.5-50 ppm			[85]
		NiO doped ITO	H_2S	0.1-100 pm			[86]
		ZnO	CO	0.5-100 ppm	< 500 ppb	0.091 °/ppm	[87]
		$Fe_2H_2O_4$	As^{3+}	0.4-10 ppb	0.6 ppb	As^{3+}: 1.092 °/ppb	[88]
Organic composites	Bio	AgNCs/Chitosan	Mouse IgG	0.6-40 μg/mL			[89]
		MIP film	Histamine	25-10^3 μg/L	25 μg/L		[90]
		Triangular AgNPs/Chitosan	Bovine IgG	7.5x10^{-2}-40 μg/mL	0.075 μg/mL		[91]
		Graphene/MIP film	L-Tryptophan	0.15-2.5 mM	0.105 mM		[92]
		AgNPs-CS-PSS-CS /GO	Beta-amylod 1-42	2-4x10^8 fM	1.21 fg/mL		[93]
		Lipase /polyacrylamide gel	Triacylglyeride	0.5-7 mM		3.17 nm/mM	[94]
	Non-bio	MIP film	Profenofos	10^{-4}-10^{-1} μg/L	2.5x10^{-6} μg/L	12.7 nm/(μg/L)	[95]
		GO/MIP film	Benzylpenicillin	1-100 ppb	0.021 ppb		[96]
		MIP film	Triclosan	0.05-1 ng/mL	0.017 ng/mL		[97]
		Pyrrole/Chitosan /ITO	Cd^{2+}	0-200 μg/L	0.129 nM	1.306 nm/(μg/L)	[98]

researchers and clinicians with a valuable platform for studying molecular interactions with high sensitivity, specificity, and real-time capabilities.

Various strategies can be employed to impose those advantages over other detection techniques, depending on the type of sensing materials. Table 2 categorizes previously reported SPR sensors based on the types of sensing materials (2D materials,[69–78] metal oxides,[79–88] organic composites.[89–98]) and analytes, and summarizes their performance.

4.1 2D materials based SPR sensors

2D materials are substances with layered structures like graphene, transition metal dichalcogenides (TMDs), and MXenes. 2D materials have been gradually applied to chemical sensors due to their own unique properties, such as large specific surface areas, optical properties, and photoelectric properties. The electron transport from 2D materials to Au film is facilitated by the lower work function of 2D materials in comparison to an Au film when applied to SPR sensors.[99] The enhanced electron density on the Au film surface amplifies the plasmonic electric wave and the evanescent wave's penetration depth. Because of its increased penetration depth, the SPR sensor responds more sensitively to changes in the refractive index of the sensing medium, leading to an increase in sensitivity. The large specific surface areas of 2D materials provide many reactive sites for interacting directly with target molecules. Furthermore, for the sensitive and selective detection of target molecules, a variety of receptors, such as antibodies, aptamers, and enzymes, are utilized. 2D materials can serve as immobilization layers for these receptors. These ultra-thin and uniform 2D materials exhibit a low damping effect as they do not interfere with the plasmonic wave of metal films.[100] Ultimately, introducing 2D materials into the SPR sensor enables selective and sensitive detection, resulting in fast response times, low cost, and simplicity to use that traditional techniques may not have shown.

4.1.1 Biosensor applications

2D materials utilizing substances produced within the body are widely employed in the field of biosensors. Biocomponents like antibodies, aptamers, and enzymes recognize and bind to specific target molecules through interactions such as the specific binding of antigens and antibodies, the complementary base pairing of RNA and DNA, or protein-protein interaction. These biocomponents are immobilized on the large surface areas of 2D materials, binding selectively to specific target biomolecules even at low concentrations. The selective capture

View Article Online
DOI: 10.1039/D4TC04800C

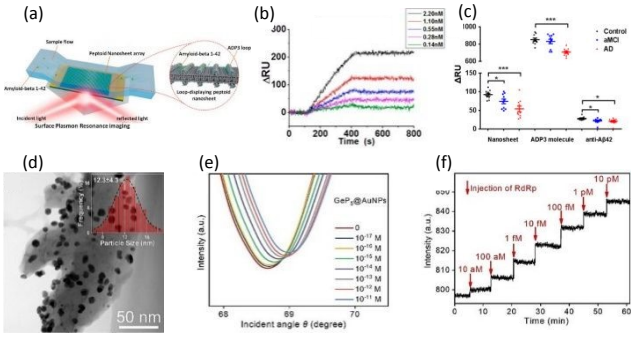

Fig. 9. (a) Schematic illustrations for the detection of $A\beta_{42}$ by the ADP3NSs. (b) Real time SPR responses for $A\beta_{42}$ at different concentrations ranging from 0.14 to 2.2 nM. (c) SPR responses with the control individuals (n=10), aMCI patients (n=10), and AD patients (n=10) using ADP3NSs, ADP3 molecules, and anti-$A\beta_{42}$. Reproduced with permission from ref. 69 Copyright © 2020 American Chemical Society. (d) TEM image of AuNPs-decorated GeP_5NSs (inset: the size distribution of AuNPs). (e) SPR spectra and (f) Real time SPR responses for RdRp at different concentrations ranging from 10^{-17} to 10^{-11} M. Reproduced with permission from ref. 70 Copyright © 2023 Elsevier B. V.

of biomolecules changes the refractive index around the sensing materials of the SPR sensor and induces the SPR signals. In addition to improving sensitivity through the electron transport, these advantages of 2D materials can significantly enhance the performance of the SPR sensor, enabling selective and sensitive detection of biomolecules even at very low concentrations.

As the global population ages faster, the problems associated with aging are getting more attention. Alzheimer's disease (AD) is one of the most common neurological disorders. For early diagnosis, the need for sensors that can distinguish between AD and amnestic mild cognitive impairment (aMCI) is rising. In order to diagnose AD, research is concentrating on sensors that can detect biomarkers, especially amyloid-beta 1-42 ($A\beta_{42}$). Gao et al. applied 2D biocomponents that can selectively bind to $A\beta_{42}$ to SPR sensors.[69] They detected $A\beta_{42}$ sensitively in the serum and plasma to distinguish between AD and aMCI through Alzheimer's disease peptoid 3 nanosheets (ADP3NSs) based SPR sensors. The amphiphilic peptoids have self-assembly characteristics through hydrophobic and electrostatic properties, making it easy to synthesize ordered ADP3NSs and form $A\beta_{42}$-binding loops on the surface. The surface-exposed loops on ADP3NSs function like the loops in an antibody that bind to a target antigen. To enhance the adsorption of $A\beta_{42}$ and restrict the nonspecific binding, Gao's group deposited uniformly distributed ADP3NSs on the surface of an Au layer and demonstrated how highly sensitive the ADP3NSs based SPR sensor is to $A\beta_{42}$ at the level of nM, changing the refractive index near the sensing materials to further induce the SPR signals (Fig. 9a). In Fig. 9b, the real-time SPR response to $A\beta_{42}$ in the concentration range of 0.14 to 2.20 nM is shown. Significant signals are observed in spite of the extremely low concentrations. After about 300-400 seconds, the specific binding between the injected $A\beta_{42}$ and ADP3NSs reach a dynamic equilibrium where the response remains constant. At even low concentrations, $A\beta_{42}$ can be detected through specific binding with ADP3 and $A\beta_{42}$ in rapid response time.

As shown in Fig. 9c, they detected $A\beta_{42}$ in serum and plasma extracted from the blood of normal individuals (n = 10) and real patients with AD (n = 10) and aMCI (n = 10) based on the different sensing materials: ADP3NSs, ADP3 molecules, and anti-$A\beta_{42}$. For three sensing materials, they observed that MCI patients had lower signals than normal individuals, whereas AD patients had much lower, evaluating the sensors' ability to distinguish between AD and aMCI and provide an accurate diagnosis. However, the signal difference among the groups was greatest in ADP3NSs, indicating that 2D ADP3NSs are most effective in distinguishing aMCI and AD. This research also demonstrated the outstanding sensitivity of ADP3NSs by showing a linear relationship between the SPR signals and $A\beta_{42}$ concentrations ranging from 1 pM to 10000 pM. As a result, the authors have demonstrated the highly sensitive and real-time SPR sensor capable of recognize $A\beta_{42}$ at incredibly low $A\beta_{42}$ concentrations. The 2D ADP3NSs SPR sensor can measure the concentration of $A\beta_{42}$ in the serum and plasma of real patients, and sensitively and accurately diagnose normal individuals, aMCI patients, and AD patients.

Covid-19, which emerged in 2019, rapidly spread worldwide, causing epidemic respiratory diseases and resulting in an immense loss of life. Due to the highly contagious nature of the virus, prompting the World Health Organization (WHO) to recommend self-isolation for infected individuals,[101] there was a crucial need for accurate and rapid diagnostics. Chang et al. introduced metallic 2D GeP_5NSs, which exhibit excellent electron transport properties in contact with Au, decorated with AuNPs on an Au layer to detect SARS-CoV-2 RNA (RdRp).[70] In addition to enhancing the plasmonic wave by transporting electrons to Au film, GeP_5NSs significantly improved the sensitivity of the sensor by strengthening the coupling between the SPR of Au film and the LSPR of AuNPs. And AuNPs immobilized complementary RdRp (cRdRp), which hybridizes with RdRp. When RdRp is injected, the cRdRp on AuNPs captures RdRp, causing fluctuations in the refractive index around the sensing materials. Then, GeP_5 and AuNPs amplify the SPR signals, leading to highly sensitive detection. Chang's group successfully assembled GeP_5NSs on the Au film by layer-by-layer technique and decorated the NSs with AuNPs facilely to assist the sensitivity enhancement. In Fig. 9d, the TEM image confirms uniformly distributed AuNPs on GeP_5NSs and the inset indicating the size distribution of AuNPs shows the average size of AuNPs is 12.3 ± 4.3 nm.

The SPR spectra for various concentrations of RdRp ranging from 10^{-17} to 10^{-11} M is shown in Fig. 9e. In the SPR spectra, the reflectance curves shifted upward and to the right as the concentration of RdRp increased. The significant increase of resonance angle and minimum reflectance was caused by the hybridization of the injected RdRp with cRdRp. The ability to exhibit linearity across an extensive range and produce a meaningful response even at a very low concentration of 1 pM shows this sensor's high sensitivity in detecting RdRp. Fig. 9f demonstrates that the proposed AuNPs/GeP_5NSs SPR sensor can be applied to the real-time monitoring for RdRp. The sensor showed a linear and real-time increase in response as the concentration continuously rose. Moreover, the sensor reached

View Article Online
DOI: 10.1039/D4TC04890C

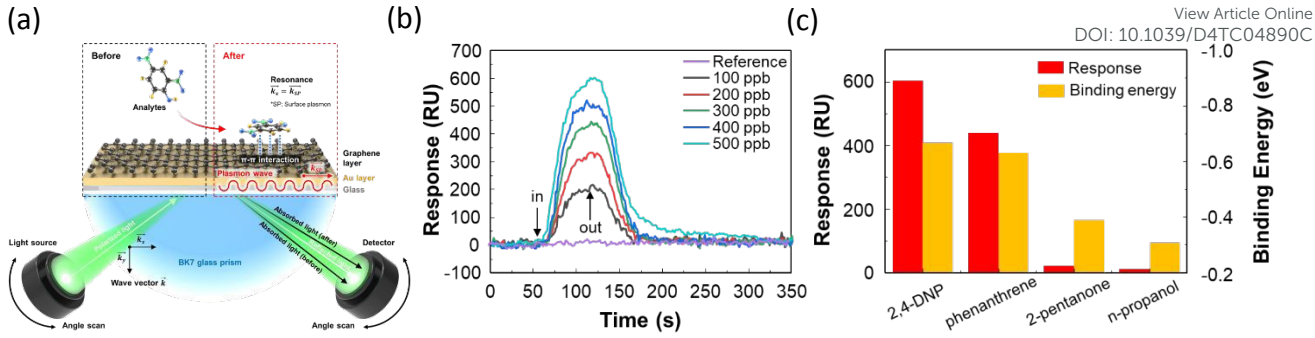

Fig. 10. (a) Schematic illustration for detection of 2,4 DNP on graphene based SPR sensor. (b) Real time SPR responses for 2,4 DNP at different concentrations ranging from 100 to 500 ppb. (c) Responses and calculated binding energies for various impurities. Reproduced with permission from ref. 77 Copyright © 2024 John Wiley & Sons.

dynamic equilibrium just within several minutes for each detection, and the time taken to reach equilibrium was consistent across all concentrations. This ultrasensitive, real-time, and rapid SPR sensor, which showed noticeable performance, is applicable for detecting RdRp and diagnosing Covid-19.

2D materials can enhance the electron density on the plasmonic metals and further improve the plasmonic electric field, leading to the enhancement of sensitivity. And the large surface areas of 2D materials provide a number of active binding sites based on immobilization of the biocomponents. As a result, the sensitivity and selectivity of SPR sensors are dramatically enhanced. 2D materials offer the potential to be applied in practical applications such as pharmaceutical research and disease diagnosis using SPR biosensors.

4.1.2 Non-biosensors applications

Graphene and its derivatives, like graphene oxide (GO) and reduced graphene oxide (rGO), are 2D materials that have large surface areas and superior physical and chemical properties compared to traditional materials like oxides and nitrides. Graphene, being composed of a single layer of carbon rings, can adsorb chemical molecules containing aromatic rings through pi-pi stacking. And GO and rGO include many functional groups, such as hydroxyl groups and ester groups, that allow them to form pi-pi stacking and hydrogen bonds with various chemicals. The large surface area of graphene, GO, and rGO maximizes the active sites to interact with chemical substances like small dye molecules, antibiotics, and pesticides. Due to these properties, the label-free and real-time 2D materials based SPR sensor can detect chemical molecules sensitively and be utilized in studying the kinetics of binding.

Isopropyl alcohol (IPA) is a solvent used for cleaning in semiconductor processing technology. Maintaining high purity of IPA is critical for increasing the overall yield of semiconductor manufacturing processes.[102] Cho et al. reported a graphene-based SPR sensor that can detect 2,4-dinitrophenol (2,4-DNP), one of the aromatic compounds that may dissolve in IPA.[77] Fig. 10a illustrates the SPR measurement system where 2,4 DNP interacts with the recognition layer, graphene. SPR signals are produced by the adsorption/desorption of 2,4 DNP on graphene through pi-pi stacking, which induces fluctuations in the local refractive index on the Au film. The authors demonstrated that 2,4-DNP, containing electron-withdrawing NO_2 groups, adsorbs onto graphene by pi-pi stacking, causing p-doping in graphene. The shift in transfer curve of solution-gated field-effect transistors and the peak shift in Raman spectra were used for evidence of this p-doping effect.[103,104] The real-time detection of 2,4-DNP is shown in the concentration range of 100 to 500 ppb (Fig. 10b). Even at very low concentrations of several hundred ppb, the SPR sensor exhibited substantial responses and outstanding quick response time and recovery time of 31 and 38 seconds, respectively. Other aromatic and non-aromatic compounds were detected by this SPR sensor at 500 ppb. The aromatic compound phenanthrene, which can strongly interact with graphene through pi-pi stacking, showed a high response, while the two non-aromatic compounds, 2-pentanone and n-propanol, exhibited no significant responses (Fig. 10c). The binding energies calculated by density functional theory confirmed a similar trend to these results.

Owing to their substantial surface area and remarkable electrical and optical properties, 2D materials exhibit strong and sensitive binding with chemical substances.[105] In particular, graphene and its derivatives, composed of carbon rings in an extensively large surface area, can effectively interact with chemical molecules containing aromatic rings, maximizing pi-pi stacking. This enables graphene and its derivatives to efficiently adsorb various molecules and produce SPR signals. The ability to enhance the plasmonic electric wave and maximize the binding with chemical molecules makes 2D materials to enable real-time detection of chemical molecules via SPR sensors and the observation of kinetic binding between 2D materials and chemical molecules. The combination of 2D materials and SPR holds broad applications in environmental monitoring, food monitoring, and chemical analysis.

4.2 Metal oxides based SPR sensors

In recent years, metal oxides have attracted a lot of interest in the field of bio-chemical sensors, owing to their biocompatibility, low-cost, and facile synthesis. Their versatility enables the development of composites containing 2D materials and organic materials, as well as the fabrication of diverse nanostructures. Metal oxides, when incorporated into SPR sensors, have multifunctionality, including enhancing sensitivity, immobilizing biocomponents, and directly binding

View Article Online
DOI: 10.1039/D4TC04890C

with target molecules. Metal oxides applied in guided wave surface plasmon resonance can strengthen the plasmonic wave and improve the sensitivity of the sensor when deposited very thinly on plasmonic metals due to their high refractive index.[106] Additionally, metal oxides can directly interact with target molecules through intrinsic oxygen vacancies or electron transfer. They can also immobilize biocomponents that selectively bind to target molecules. The binding of target molecules to metal oxides or biocomponents on metal oxides induces changes in the refractive index around the sensing materials, resulting in the generation of SPR signals.

4.2.1 Biosensor applications

Various biomarkers, including neurotransmitters, hormones, and metabolites, are detected by several analyses to diagnose diseases. Traditional methods that have been researched for selective detection of biomarkers have critical limitations. Fluorescent sensors require labelling target molecules, and liquid chromatography is time consuming for detection.[107,108] Recent research is actively underway on real-time SPR sensors, enhanced by deposition of metal oxides to improve sensitivity and selectively detect target molecules.

Among metabolites, xanthine is one of the intermediate compounds occurring during the metabolism of purine nucleotides. Since xanthine is converted into uric acid by the xanthine oxidase (XO) enzyme, the concentration of xanthine serves as an indicator for pathological diseases such as gout, hyperuricemia, cerebral ischemia, perinatal, and tumor hyperthermia.[109] Kant et al. reported a sensitive and selective SPR sensor for xanthine by depositing Ta_2O_5 nanofibers (Ta_2O_5NFs) and immobilizing XO enzymes on a Ag layer (Fig. 11a).[80] They enhance the plasmonic wave and further improve sensing performance by depositing a thin film of high refractive index Ta_2O_5NFs onto an Ag film. Additionally, they immobilized XO enzymes on the surface of sensing material, selectively decomposing only xanthine and inducing changes in the refractive index around the sensing material. The combination of these two effects resulted in the development of a highly sensitive and selective sensor for xanthine.

In Fig. 11b, to validate the selectivity of the XO enzymes, three interferents were compared with respect to shifts in the resonance wavelength. Interferants such as caffeine, glucose, and ascorbic acid showed negligible shifts of less than 10 nm, whereas xanthine showed a significant shift of over 40 nm. These specific recognition and decomposition of enzymes are suitable for application in SPR sensors for sensitive and selective detection. Fig. 11c illustrates the real-time SPR response of the XO/Ta_2O_5 based sensor. The change of the transmission intensity (λ= 617.5 nm) before and after the injection of 3 μM xanthine clearly shows that the response decreased and saturated within one minute after the injection. Furthermore, the response recovered to its original value and stayed steady one minute after xanthine was removed. This indicated that both the response time and recovery time are less than one minute, implying that the proposed SPR sensor is very fast and able to detect in real time.

Kant et al. improved the sensing performance by depositing a high refractive index metal oxide, enhancing the plasmonic electric wave. They also immobilized enzyme on metal oxide. As a result, the sensor's sensitivity and selectivity are remarkable, and rapid response time and recovery time make it highly suitable for the practical application of disease diagnosis.

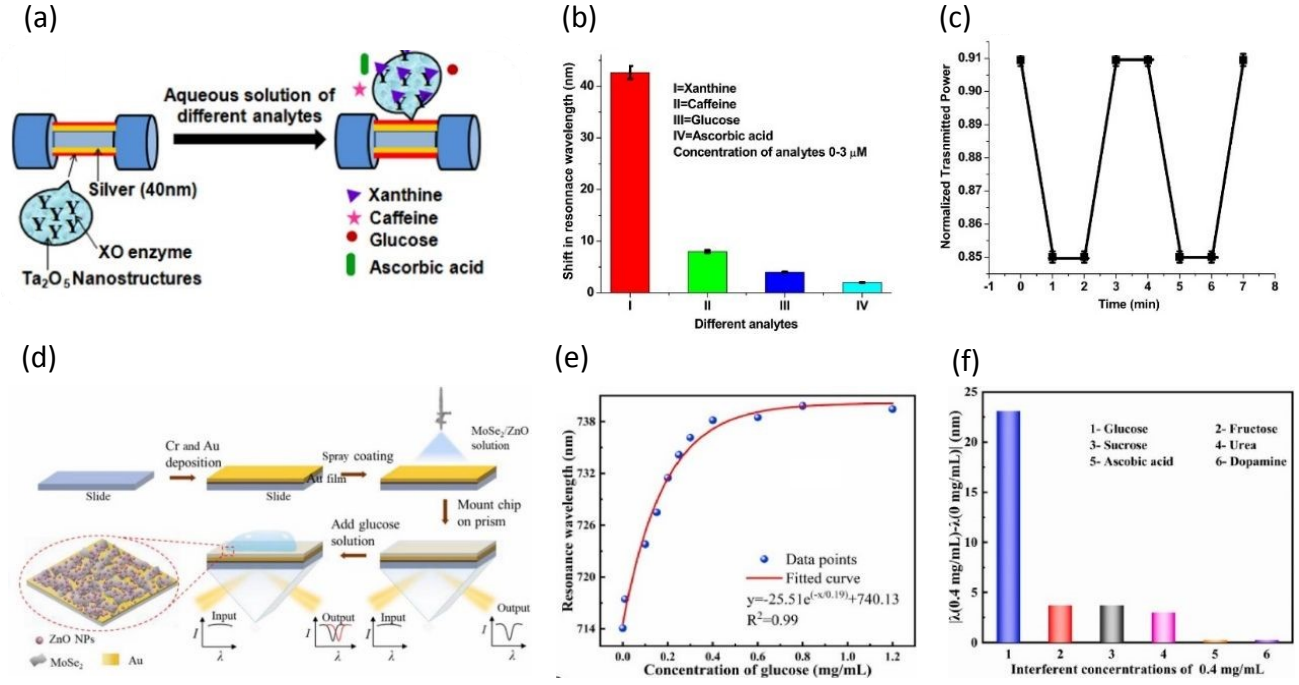

Fig. 11. (a) Schematic illustration for detection of Xanthine on XO enzyme entrapped Ta_2O_5 NFs based SPR sensor. (b) Resonance wavelength shifts compared with interferents. (c) Real time SPR responses for 3 μM Xanthine. Reproduced with permission from ref. 80 Copyright © 2017 Elsevier B.V. (d) Schematic illustration of fabricating the $MoSe_2$/ZnO-based SPR chips. (e) The resonance wavelength shifts for Glucose at different concentrations ranging from 0 to 1.2 mg/mL. (f) Selectivity analysis with 0.4 mg/mL interferents. Reproduced with permission from ref. 79 Copyright © 2023 Elsevier B.V.

View Article Online DOI: 10.1039/D4TC04899C

One of the most significant indicators of health management is glucose, which is especially relevant for diabetes. The real time measurement of blood glucose levels is necessary for maintaining blood glucose levels within the normal range and diagnosing diabetes.[110] Outside the care of diabetes, there is medical and biological research,[111] food monitoring,[112] and systematic training for athletes,[113] all of which are greatly correlated with the prompt and accurate detection of glucose. Chen et al. introduced ZnONPs/$MoSe_2$NSs composite film to the SPR sensor for glucose detection without utilizing enzymes.[79] Fig. 11d illustrates the simple procedure for preparing the non-enzymatic ZnONPs/$MoSe_2$NSs based sensor. The sensor chip was fabricated by spray coating ZnONPs/$MoSe_2$NSs composite solution onto an Au film. ZnONPs in the sensing layer can bind to glucose through chemisorption on their surface, inducing fluctuations in the refractive index. Furthermore, ZnONPs can easily form composites with $MoSe_2$NSs which have large surface areas and outstanding electrical properties. This can be achieved by simply dissolving them in an organic solvents and heating. The composite film of ZnONPs and $MoSe_2$NSs recognized and bound to glucose sensitively and selectively without enzymes and amplified the signals.

With the non-enzymatic ZnONPs/$MoSe_2$NSs based sensor, the authors detected glucose in the concentration range of 0 to 1.2 mg/mL (Fig. 11e). Under optimized conditions, the sensor exhibited a total wavelength shift of 25.75 nm for the glucose range of 0 to 1.2 mg/mL. Furthermore, this optimized sensor demonstrated the linearity within the range of 0 to 0.3 mg/mL, the sensitivity of 72.17 nm/(mg/mL), and the calculated limit of detection (LOD) of 0.023 mM. This highly sensitive performance is comparable to previously reported enzyme-based sensors favorably. Because of their similar structures and properties to glucose, fructose, sucrose, urea, ascorbic acid, and dopamine are significant interferents in actual glucose detection applications. Fig. 11f illustrates the resonance wavelength shifts for the interferents and glucose at 0.4 mg/mL. The resonance wavelength shifts for fructose, sucrose, and urea are 3.75 nm, 3.8 nm, and 2.41 nm, respectively. And the shifts for ascorbic acid and dopamine is less than 1 nm. All of these shifts are negligible in comparison to the large shift generated by glucose, indicating the excellent selectivity of the non-enzymatic ZnO NPs/$MoSe_2$ NSs based sensor.

A highly sensitive and selective ZnO/$MoSe_2$ based glucose sensor without enzymes was reported by Chen's group. ZnONPs bind to glucose, and $MoSe_2$ NSs enhanced the sensitivity of the sensor. With a LOD of 0.023 mM and a sensitivity of 72.17 nm/(mg/mL) in the linear range of 0 to 0.3 mg/mL, the sensor performed excellently not only in detecting glucose but also in exhibiting good selectivity against five interferents. With its performance, this sensor has demonstrated its potential to be applied as a biosensor in medical diagnostics, bio-medical research, and food monitoring.

Depositing a thin layer of high refractive index metal oxide onto a plasmonic metal can enhance the plasmonic wave, thereby improving the sensing performance. Additionally, the characteristics of metal oxides, such as their ability to form composites easily with other substances, along with their intrinsic features like oxygen vacancies and electron transfer for direct interaction with target substances, contribute to enhancing the binding with target molecules. With these effects, metal oxide based SPR sensors can rapidly, sensitively, and selectively capture target molecules. Such sensors are expected to find widespread use in fields demanding highly sensitive, label-free, and real-time sensing capabilities, such as healthcare devices and medical research.

4.2.2 Non-biosensor applications

Metal oxides, particularly those like WO_3, SnO_2, and TiO_2, are extensively used in the field of gas sensors.[66,114–116] These metal oxides interact with toxic gases such as hydrogen, acetone, ammonia, and NO_2, enabling their detection. Numerous studies have shed light on the interaction between gas molecules and metal oxides like chemisorption. Therefore, metal oxides can be applied to SPR sensors, allowing for the real-time and highly sensitive detection of gas molecules, even at very low concentrations.

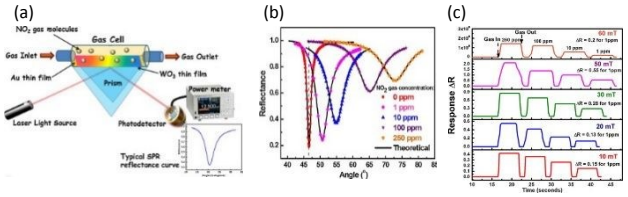

Fig. 12. (a) Schematic of the SPR gas sensing measurement. (b) SPR spectra for NO_2 gas at different concentrations from 0 to 250 ppm. (c) Real time SPR responses for the sensors having WO_3 thin films grown at different pressure with repetitive exposure of NO_2 gas of different concentrations ranging from 1 to 250 ppm. Reproduced with permission from ref. 85 Copyright © 2015 Elsevier B.V.

Among the toxic gases, NO_2 is a serious air pollution gas that can cause significant health issues for humans.[117] In the last decades, various sensors have been developed to detect NO_2, including colorimetric sensors,[118] chemoresistive sensors,[119] and surface acoustic sensors,[120] However, all of these sensors have certain shortcomings, such as low sensitivity, excessive power consumption, or sluggish response time. However, because of the high sensitivity, low power consumption and fast response time, SPR sensors that incorporate metal oxides have become a promising technology for NO_2 detection. Most importantly, metal oxide based SPR sensors are particularly suitable for applications such as industrial safety monitoring and environmental monitoring, where real-time detection of hazardous gases like NO_2 in room temperature is critical. This has led to ongoing research on the SPR sensors for the accurate and efficient NO_2 monitoring in various environments. Paliwal et al. proposed a SPR sensor with WO_3 thin film as the sensing material for NO_2 detection at room temperature.[85] Considering the properties of SPR sensors where gas detection occurs on the sensor's surface, WO_3 film was deposited onto an Au layer through RF-magnetron sputtering at different growth pressures in order to control grain boundaries and surface roughness. Fig. 12a illustrates the SPR gas sensing measurement. They suggested a mechanism for NO_2 detection based on the change in the refractive index of WO_3 due to the adsorption of NO_2. The

View Article Online
DOI: 10.1039/D4TC04890D

mechanism is related to the refractive index changes of the WO_3, based on the adsorption of NO_2. As an oxidizing gas, NO_2 takes electrons from WO_3 forming either NO_2^-, NO, or O^- then NO_2^- and O^- adsorbs onto the surface of WO_3. The refractive index of the WO_3 changes as a result of electron loss and adsorption of NO_2^- and O^-, leading to the generation of SPR signal.

Fig. 12b shows the SPR spectra at different concentrations from 0 to 250 ppm of NO_2 for the sensor fabricated under the optimized condition. As the concentration of NO_2 increases, it is found that the resonance angle and the minimum reflectance increase, and the curves become broader. The huge shift in resonance angle with concentration indicates that the mechanism mentioned above is valid. Furthermore, the significant changes in resonance angle and minimum reflectance demonstrate that this sensor is highly sensitive and effective for NO_2 detection. The pink curve in Fig. 12c represents the real-time SPR responses based on the reflectance changes of the sensor fabricated under the optimized condition. The responses saturate in less than 2 seconds when NO_2 is injected for every measured concentration. As the air is reinjected for recovery, the responses also return to their original values within 2 seconds. The rapid response and recovery times achieved when detecting at room temperature are notably fast, comparable to or even faster than traditional methods measured at elevated temperatures. These advantages make the WO_3 based SPR sensor a highly suitable method for real world, where rapid detection of hazardous gases is essential. Furthermore, after repetitive detection of NO_2, there is no discernible change in the baseline. All of these results confirm the high sensitivity of the WO_3 based SPR sensor reported by Paliwald's group, along with its very fast response and recovery time, real-time detection capability, and good stability, attributed to the physical and chemical adsorption of NO_2 taking electrons from WO_3.

Metal oxides are inexpensive, easy to make nanostructures, and can synergize with other materials, making them suitable for the detection of chemical substances like gas molecules in SPR sensors. Metal oxides can adsorb chemical molecules physically and chemically either through their intrinsic oxygen vacancies or direct electron transfer. Compared to previously reported sensors, metal oxide-based SPR sensors exhibit significantly faster response and recovery times along with higher sensitivity. Furthermore, metal oxide-based SPR sensors have exceptional properties for repeatability and long-term stability due to the inherent stability of metal oxides. As a result, metal oxide based SPR sensors can be widely applied in the fields of industrial safety monitoring, environmental monitoring, and water quality management.

4.3 Organic composites based SPR sensors

Organic composites refer to materials formed by the combination of organic molecules, which are composed of carbon skeletons and other elements such as H, O, and N, with other substances such as other organic molecules, metals, metal oxides, nitrides, and so on. Organic composites are employed in constructing sensing materials to uniformly distribute metal NPs and reactive materials that interact with target molecules to enhance the plasmonic electric field and increase active sites. Additionally, organic composites are also utilized in the formation of molecular imprinting polymer (MIP) films which provide specific binding sites for target molecules. The MIP film method is a technique for forming sensing materials by mixing and polymerizing the target molecule with other organic molecules. After depositing uniform polymer film, the target molecules are eliminated, creating the imprinted sites on the surface of the sensing material. The created vacant sites can only adsorb the target molecules highly selectively and sensitively, leading to a fluctuation in the refractive index around the sensing material and generation of SPR signals. Due to these capabilities, researchers have employed many organic composites for composing the sensing materials in the fields of environmental monitoring, biomedical research, and biosensors.

4.3.1 Biosensor applications

Organic composites can be synthesized by simply mixing various substances, including organic molecules, and polymerizing them. The combination of organic molecules with various functional groups can result in a variety of organic composites. Particularly, fixing organic molecules on the surface of metal NPs can prevent the aggregation of NPs, allowing for a uniform film to be produced through a subsequent spin coating process. When plasmonic metal NPs are evenly distributed on a plasmonic metal film, the interaction of plasmonic electric fields between plasmonic metal NPs and the plasmonic metal film can be amplified, leading to enhanced sensitivity. In the context of sensors detecting biomolecules, the use of biocomponents to form specific bindings is common. However, if the immobilization layer's quality has an impact on repeated measurements, sensor performance can gradually deteriorate as the fixed biocomponents separate over time. In such cases, forming a MIP film through organic composites can enable the development of a sensor capable of specific binding even without biocomponents, ensuring long-term stability.

Immunoglobulin G (IgG) is one of the antibodies found in the body fluids of humans and other mammals. IgG binds to specific viruses or bacteria to neutralize their toxicity, and it modulates various immune responses within the immune system.[121] It is essential for regulating immunological reactions. Prior to human trials, studies with mice are frequently carried out to evaluate stability and safety.[80] As a result, there is a growing interest in the sensitive detection of mouse IgG with the increasing demand for mouse IgG. Zhang et al. reported a SPR sensor fabricated using Ag nanocubes (AgNCs)/chitosan composites as sensing materials (Fig. 13a).[89] They used organic molecules to produce composites of AgNCs, glutaraldehyde, and chitosan, which were spin-coated onto the Au layer. This composite involved the binding of 3-Mercaptopropinic acid (MPA), an organic molecule, with thiol functional groups to AgNCs, forming Ag-S bonds. This process successfully prevented the oxidation of AgNCs. Additionally, the researchers aimed to

View Article Online
DOI: 10.1039/D4TC04890C

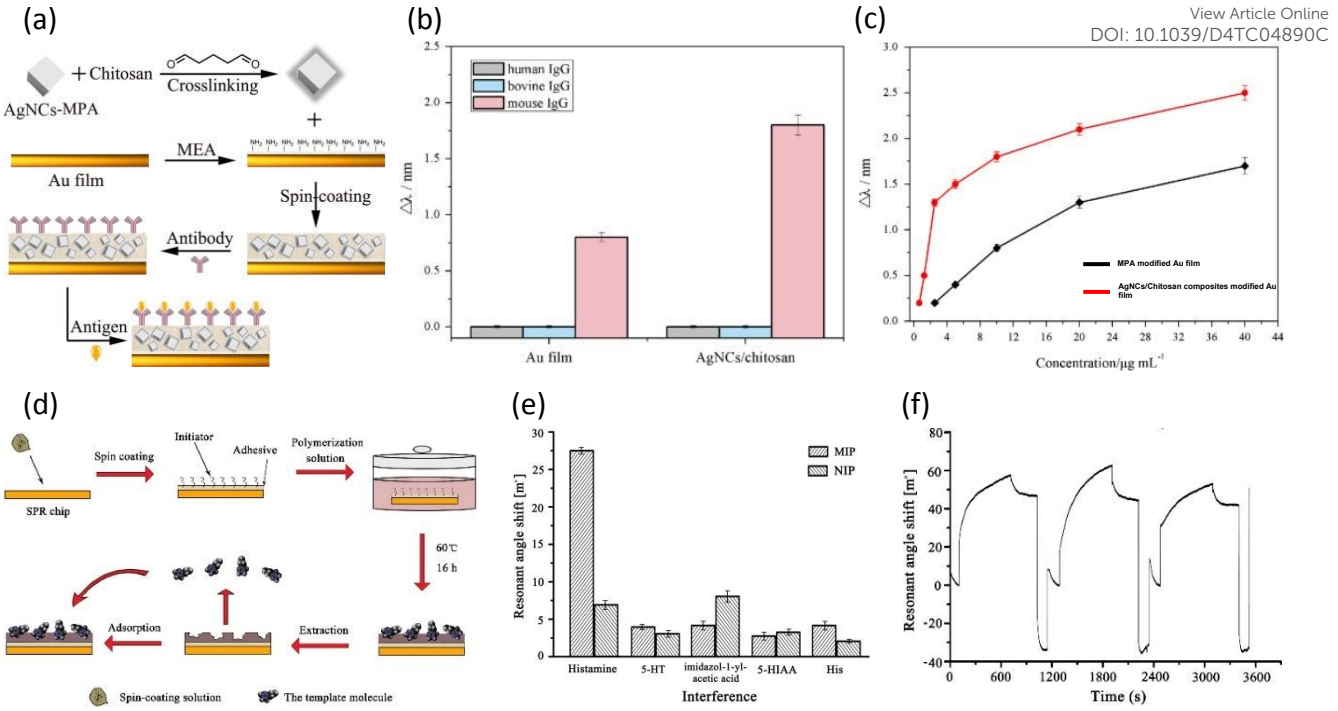

Fig. 13. (a) Schematic diagram for fabrication of the TSNPs/chitosan composites based SPR sensor. (b) Resonance wavelength shifts for interferents on different sensing layers. (c) Resonance wavelength shifts for Mouse IgG at different concentrations ranging from 0.6 to 40 μg/mL. Reproduced with permission from ref. 89 Copyright © 2015 Elsevier B.V. (d) Schematic illustration of fabricating Histamine imprinted polymer based SPR sensor. (e) Resonance angle shifts compared with interferents on MIP and NIP. (f) Real time and repetitive SPR responses for 500μg/L histamine. Reproduced with permission from ref. 90 Copyright © 2015 Elsevier B.V.

enhance the sensitivity by spreading AgNCs very uniformly and thinly onto the Au layer, promoting interaction between the plasmonic electric fields of AgNCs and Au film. Then, they immobilized the antibodies for mouse IgG on the surface of the composite film by flowing a solution containing the antibodies. Through Schiff alkali reaction with aldehyde groups of glutaraldehyde, the injected antibodies could be bound. Subsequently, when flowing mouse IgG solution, the immobilized antibodies strongly bind to mouse IgG through antigen-antibody interaction, causing the shifts of resonance wavelength.

Fig. 13b compares the resonance wavelength shifts for three different IgGs on both MPA modified Au film SPR sensor and the AgNCs/chitosan based SPR sensor after immobilizing same antibodies on their surfaces. Both sensors showed extremely specific binding to mouse IgG, demonstrating the selectivity of the antibodies utilized in mouse IgG detection. And the sensitivity of both sensors to mouse IgG was twice as high in the AgNCs/chitosan layer compared to the MPA modified Au layer. This shows the effectiveness of the proposed AgNCs/chitosan layer in enhancing the sensitivity of the SPR sensor, emphasizing its impact on improving sensitivity in mouse IgG detection. Fig. 13c illustrates the resonance wavelength shifts for the AgNCs/chitosan composites based sensor and MPA modified Au film sensor with respect to mouse IgG concentrations ranging from 0.6 to 40 μg/ml. Before initiating the detection of mouse IgG, ethanolamine hydrochloride was used to ensure specific binding to the surface of sensing materials. The AgNCs/chitosan based sensor exhibited a resonance wavelength change of 2.50 nm in the detection range, and the calculated minimum detectable concentration was four times lower compared to the MPA modified sensor. It has been shown that uniformly dispersing AgNCs on the Au layer via AgNCs/chitosan composites improved the plasmonic electric wave of the Au layer and, consequently, SPR signals.

Histamine, an organic nitrogen compound, serves as a neurotransmitter and actively participates in immune system functions. This small molecule can be found in tissues like white blood cells and the nervous system. The accurate detection of histamine is crucial in the fields of medicine, pharmaceuticals, and biotechnology for diagnosing neurological and immunological disorders and developing pharmaceuticals. Jiang et al. prepared MIP film based SPR sensor for highly sensitive, selective, and reliable detection of histamine.[90] They used the polymerization of a solution containing histamine and other organic molecules. Subsequently, histamine was removed to form empty sites on the surface (Fig. 13d). Histamine can selectively bind to the empty sites during the measurement. At even low concentration, histamine binds to the sites, sufficiently changing the refractive index around the sensing material to generate signals.

Resonance angle shifts were measured for histamine and four interferents to assess the selectivity of MIP film for histamine, using both MIP film based sensors and non-imprinting polymer (NIP) film based sensors (Fig. 13e). The NIP film based sensor exhibited resonance angle shifts below 10 m° for all five molecules including histamine, indicating that the NIP film did not sensitively interact with any of the molecules. On the other hand, the MIP film based sensor showed shifts below 10 m° for four interferents, while histamine showed a significant

View Article Online
DOI: 10.1039/D4TC04890C

shift of approximately 27 m°. Considering the concentration differences between the measured histamine (0.1 mg/L) and interferents (10 mg/L), it was confirmed that the selectivity and sensitivity of the MIP film for histamine is substantial. The real-time SPR responses for three successive 500 µg/L histamine detections are shown in Fig. 13f. After each histamine detection, the regeneration process with 0.1 M HCl solution was conducted to detach histamine from the sensing material. The small differences in resonance angle shifts for each detection confirm the repeatability of this sensor. The resonance angle reached its maximum point within approximately 600 seconds for each detection, highlighting the real-time detection capability of the proposed sensor. The histamine MIP film based sensor, as validated by the authors for its selectivity, sensitivity, real-time monitoring, and repeatability, demonstrated the selective binding of histamine to the imprinted sites. It is anticipated to have a significant impact on researchers and pharmaceutical companies engaged in studies related to histamine.

Various organic composites, such as well-dispersed metal NPs layers and MIPs, are being utilized in SPR sensors to enhance sensitivity and selectivity. Unlike previous technologies for detecting biomolecules, these sensors do not require labels and can be easily measured with simple equipment, eliminating the need for specialized personnel. Moreover, their rapid response time and real-time measurement capabilities make organic composite-based SPR sensors applicable in various fields, including disease diagnosis, pharmaceutical research, and medical studies.

4.3.2 Non-biosensors applications

Selectively detecting chemical molecules with similar structures and characteristics is quite a challenging undertaking. MIP films of organic composites are the most extensively used materials to overcome this challenge. Through a simple polymerization of organic molecules, the target molecules are easily imprinted on the surface of the sensing material. The resulting sensing material shows repeatability through a regeneration process. These materials allow for the selective and repeatable detection of molecules in chemical sensors.

Organophosphorus pesticides (OPPs) have been used to kill pests when growing cotton, vegetables, cereals, and other crops. Even at very low concentrations, OPPs can cause serious neurological diseases in human and these are a major problem for environmental and aquatic organisms because of their comparatively high environmental mobility in water.[122] Consequently, there is a critical need for rapid and reliable detection of OPPs. Previously reported methods for detecting OPPs have difficulties such as insufficient selectivity, requirement for labels, and limitation for real-time monitoring. To overcome these difficulties, research is ongoing to develop approaches that can detect OPPs selectively in real-time and label-free. Shrivastav et al. presented an SPR sensor that employed the MIP film to detect the hazardous chemical profenofos, one of the most widely used OPPs.[95] The MIP film involves incorporating the target molecule to be detected into the sensing material using organic composites and then removing it, consequently leaving the imprinted sites on the surface of sensing material (Fig. 14a). Other molecules cannot bind to the imprinted sites and only profenofos binds to the

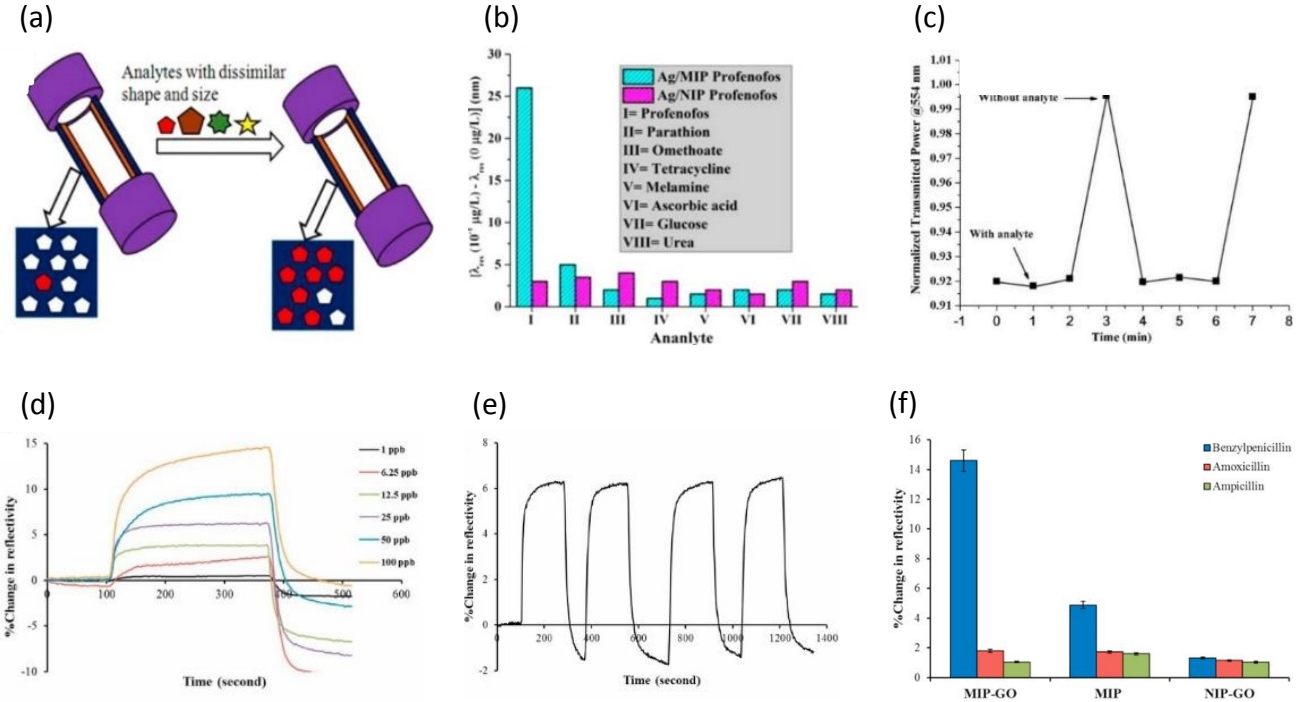

Fig. 14. (a) Schematic illustration of the high selective and sensitive profenofos imprinted sensor. (b) Resonance wavelength shifts compared with interferents. (c) Real time SPR responses for 10^{-4} µg/L profenofos. Reproduced with permission from ref. 95 Copyright © 2015 Elsevier B.V. (d) Real time SPR responses for benzylpenicillin at different concentrations ranging from 1 to 100 ppb. (e) Repetitive SPR responses for 25 ppb benzylpenicillin. (f) The reflectance changes compared with interferents on different sensing layers. Reproduced with permission from ref. 96 Copyright © 2022 Elsevier B.V.

sites strongly.

In Fig. 14b, to validate the effectiveness of MIP film, the authors observed the resonance wavelength shifts of an Ag based SPR sensor using MIP film and an Ag based SPR sensor using NIP film in response to 0.1 μg/L profenofos and other interferents. The Ag/NIP sensor without imprinted sites for profenofos showed similar small shifts for profenofos and other interferents. This confirms that the sensor lacks distinct selectivity and does not respond sensitively to profenofos in the absence of the imprinted sites. On the other hand, the profenofos-imprinted Ag/MIP sensor responded to the profenofos intensively, exhibiting a notable shift. It showed a clear difference from seven interferents, indicating good selectivity. In the Ag based sensor with MIP film, profenofos can attach firmly and selectively while interferents have minimal binding on the imprinted sites of the film. The real-time SPR response for 0.0001 μg/L profenofos is shown in Fig. 14c. The transmitted intensity at λ= 554 nm was observed with and without profenofos, where profenofos was injected for 2 minutes, followed by a minute removal of profenofos. This process was repeated twice to validate repeatability of the real-time sensor. Upon the removal of profenofos, there is a significant change in transmission in about one minute. After one minute of another profenofos injection, the response remained constant and stabilized. These results demonstrated that the sensor can detect profenofos selectively and rapidly in real-time through multiple cycles. The exceptionally fast and selective real-time detection capabilities make the MIP based SPR sensor reported by Shrivastav's group promising for applications in environmental monitoring.

Antibiotics are drugs that support the immune system in both humans and animals by decreasing the pathogens' activity when they are infected. Proper use and disposal of antibiotics can prevent the invasion of pathogens early on, allowing the host to overcome the crisis with mild symptoms such as a cold and cough. However, improper disposal can lead antibiotics to flow into the ecosystem, producing antibiotic-resistant bacteria and causing a serious problem.[123] Thus, it is essential to develop sensors that can detect antibiotics in real-time that are still present in food and water. Celik et al. reported a SPR sensor with a sensing layer consisting of a GO based MIP film to detect benzylpenicillin, one of the most widely used β-lactam antibiotics.[96] Through the specific binding of benzylpenicillin in MIP film, the sensor can selectively detect benzylpenicllin. Additionally, GO, a 2D material with excellent electrical and optical properties, was used to amplify the signals from the binding of the target molecule on the imprinted sites. GO possesses a lower work function than Au, and the electron transfer from GO to Au improves the sensitivity of the SPR sensor.[124]

Fig. 14d shows the real-time responses of the MIP-GO based SPR sensor to benzylpenicillin at various concentrations ranging from 1 to 100 ppb. The responses stabilized several hundred seconds after the injection of benzylpenicillin, and the sensor exhibited exceptional sensitivity even at ppb levels. While saturation was achieved within 100 seconds up to 50 ppb, concentration of 100 ppb showed a steady increase in response even after 100 seconds. Overall, as the concentration increases, more binding events occur, leading to a longer time to be saturated. However, the comparable fast response time up to 50 ppb confirms rapidly detect benzylpenicillin in real-time. After that, the repeatability study of the MIP-GO based sensor was measured (Fig. 14e). Four successive detections were conducted for 25 ppb benzylpenicillin, and for each detection, 10 mM NaCl was flowed through to desorb benzylpenicillin from the imprinted site. Because there was no additional stabilizing process after each detection, the reflectance changes began with negative values after the initial detection. But the reflectance changes remained at approximately 6 % for the four detections. These constant responses demonstrated that there is no degradation in the binding capacity between MIP and benzylpenicillin even after several adsorption and desorption cycles, thereby confirming the potential of the proposed sensor. Simultaneously, Celik's group conducted comparative experiments using three types of sensing materials and two interferents to demonstrate the improved sensitivity and selectivity achieved through GO and MIP (Fig. 14f). By comparing the GO-NIP-based sensor, which lacked the imprinted sites and exhibited low responses for all three substances, with the GO-MIP based sensor, which possessed the imprinted sites and showed exceptionally high response only to benzylpenicillin, the selectivity of the MIP film for benzylpenicillin was confirmed. Furthermore, the comparison between the GO-MIP based sensor and the MIP-based sensor revealed that, while both exhibited selectivity for benzylpenicillin, the presence of GO resulted in enhanced sensitivity. Celik's group reported that the GO-MIP based SPR sensor can detect benzylpenicillin rapidly in real-time by amplifying the selective but weak signals from MIP.

Utilizing the molecular imprinting films, organic composites, become highly effective when there are numerous interferents in the detection environment that may hinder the detection of target chemical molecules. The MIP films can selectively and sensitively capture target molecules due to the presence of imprinted sites. The requirement to immobilize biocomponents for selective detection is removed, lowering the possibility of biocomponents detachment throughout the procedure. This approach can be easily carried out by simply mixing organic molecules and target molecules and then removing the target molecules. Combining organic composites with SPR sensors, which enable real-time, label-free, and selective detection, holds great potential for applications in environmental monitoring, disease diagnosis, and pharmaceutical research.

5. Practical Applications of LSPR and SPR sensors

The significance of real-world applications of LSPR and SPR sensors stems from their positive impact on many scientific, industrial, and medical areas. In practical applications, these sensors allow for real-time detection of molecular interactions, providing essential insights into biological, chemical, and environmental processes. In healthcare, LSPR and SPR sensors are crucial in drug discovery, medical diagnostics, and biomolecular interaction monitoring, all of which contribute to

View Article Online
DOI: 10.1039/D4TC04890C

advances in precision medicine. Environmental monitoring benefits from the ability to identify pollutants and toxins with high sensitivity. These sensors are used in industrial settings for quality control, process monitoring, and detecting trace contaminants. The real-world application of LSPR and SPR sensors promotes developments in a variety of sectors by providing efficient and dependable instruments for monitoring and analysis, eventually boosting innovation, improving research outcomes, and improving diagnostic and decision-making processes.

Coskun et al. presented a microfluidics based plasmonic biosensing system that combines plasmonic microarrays with dual color lens-free imaging.[125] This system allows for real-time and multiplexed monitoring of binding events over a large field-of-view (>20 mm^2) in low resource settings. This platform uses an optoelectronic sensor (complementary metal-oxide-semiconductor) to record diffraction patterns of plasmonic nanoapertures at the bottom of a microfluidic channel, as

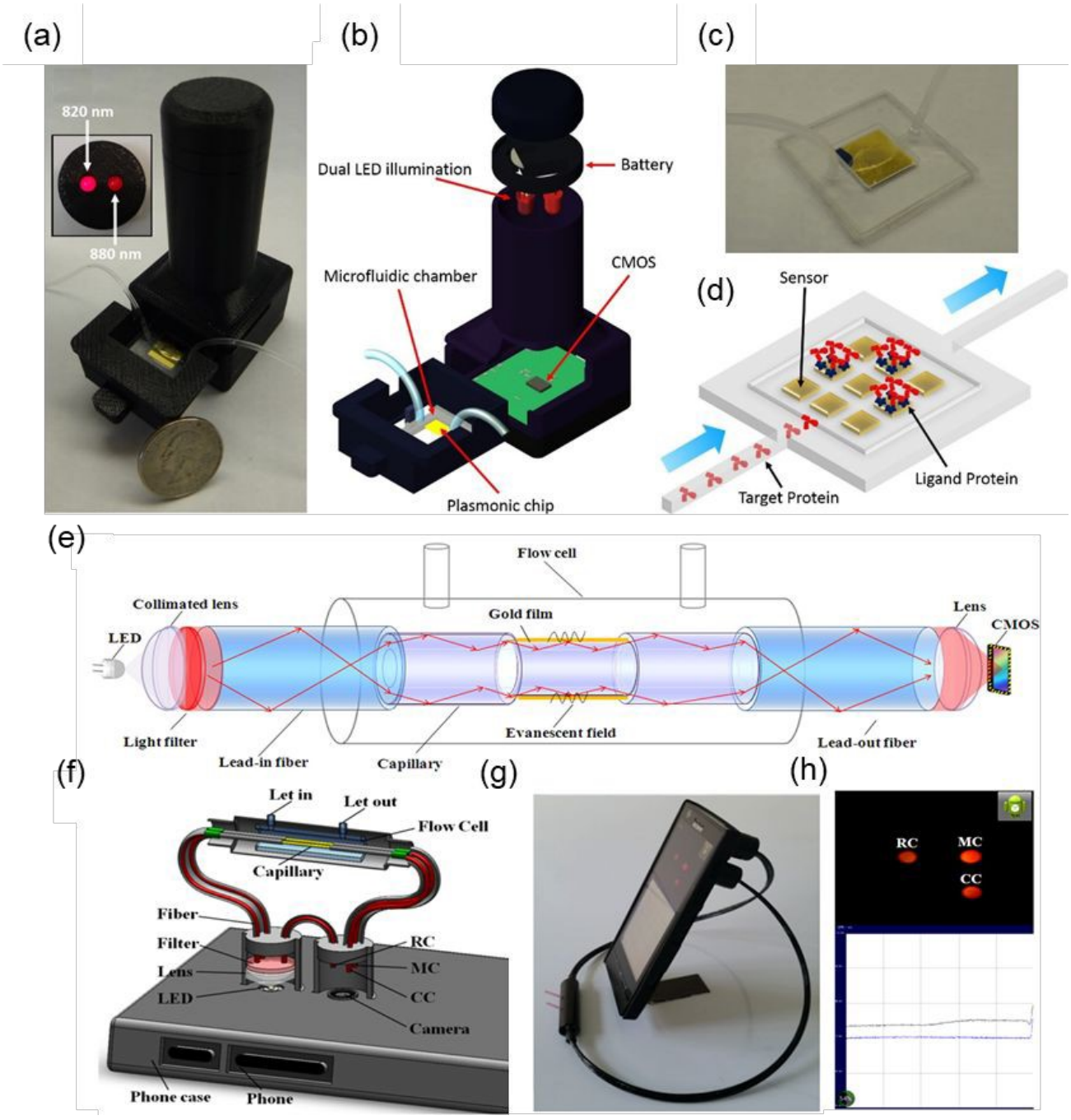

Fig. 15. (a) Photograph and (b) illustration of the LSPR sensing device which employs (c) microfluidic channel. (d) Schematic illustration of the sensing mechanism of microfluidic channel. (b) The LSPR peak of SA-Ag composite in aqueous solution of 1000 ppb of Hg^{2+}. Reproduced with permission from ref. 125 Copyright © 2014 Springer Nature. (c) Pb^{2+} Sensing mechanism of functionalized AuNPs. Schematic illustration of (e) smart phone-based SPR sensor and (f) the internal structure. Photograph of (g) the SPR sensor installed on a smart phone and (g) the smart phone of the measurement channel. Reproduced with permission from ref. 126 Copyright © 2015 Springer Nature.

View Article Online
DOI: 10.1039/D5TC04890C

shown in Fig. 15a-c. This allows for controlled delivery of target solution to surface-functionalized nanosensor arrays. Fig. 15d shows that ligand proteins functionalize plasmonic pixels to capture target proteins. The biosensing device employs a plasmonic nanohole array with excellent light confinement and nanoscale field improvements, resulting in high sensitivity to surface conditions. Changes in the refractive index near the sensor surface cause a shift in the peak wavelength of the plasmonic mode supported by the nanohole array.

Liu et al. presented a flexible, compact dual-channel SPR system.[126] Fig. 15e and h displays a schematic diagram, an photograph, and the running interface of the detection system. Since all components are attached to the phone case on the back of the smartphone (Fig. 15f), the touch-screen interface and display remain unaffected during the detecting process, as shown in Fig. 15g and h. The sensor components and the smartphone can be readily combined into an instrument and dismantled after the measurement.

6. Challenges and future perspectives

LSPR sensors rely on morphological changes in plasmonic metal NPs, while SPR sensors monitor changes in the refractive index around metal films. Although both sensors demonstrate high sensitivity to trace concentrations of analytes, they are vulnerable to environmental interferences. The environmental factors, such as temperature changes and vibrations near the sensors, generate background noise, which is further deteriorated by non-specific adsorption. This undesirable noise increases LOD, reduces sensitivity and selectivity, and eventually degrades the overall sensor performance. Therefore, addressing these challenges is crucial for improving sensor reliability and practical applicability.

In particular, the synthesis of metal NPs with uniform size and shape at the nanoscale is challenging for LSPR sensors. Since their detection mechanism is based on morphological changes, ensuring a uniform distribution of homogeneous metal NPs produces consistent and strong plasmonic resonance frequency, leading to distinct shifts in the absorption peak and noticeable color changes.[127,128] Any variation in the size, shape, or spatial arrangement of fabricated NPs dispersion can reduce detection accuracy and reproductivity. Advancements in precise synthesis techniques and complementary strategies are essential for reliable detection.

In addition to background noise, SPR sensors are also limited by sensing materials that are either thicker than the effective detection region or cause optical loss at the resonance wavelength. The evanescent wave, SPP, generated on the metal surface can only penetrate a few hundred nanometers above the metal film.[129] Refractive index changes occurring beyond this detection region are difficult to detect. Moreover, the incident light required to excite a plasmonic wave typically falls within the visible or infrared range. If sensing materials that strongly absorb light in this wavelength range are deposited on the metal film, the intensity of the excited SPP decreases, significantly weakening the SPR signals. To overcome these problems, depositing ultra-thin sensing materials with suitable optical characteristics is one of the most important considerations in developing SPR sensors.

Table 3. General advantages and disadvantages of sensing materials utilized in LSPR and SPR sensor applications.

Sensor type	Material type	Advantages	Disadvantages
LSPR sensors	Metal NPs	• Even slight morphological changes in size and shape can significantly affect the plasmonic resonance frequency • High surface-to-volume ratio to maximize interactions with analytes	• Difficulty in fabricating metal NPs with uniform size and shape
	Bimetallic NPs	• Improved stability and sensitivity due to the synergistic effect of each metal • More flexible tunability in morphology • Detection with the naked eye through multicolour changes	• Difficulty in fabricating bimetallic NPs with uniform size and shape
	MOMs	• Selective binding to analytes via surface functionalization of metal NPs • Reversible detection is possible by capping the surface of metal NPs to prevent their dissociation.	• Poor reproducibility and long-term stability due to degradation of surface functionalization
SPR sensors	2D materials	• Enhancement of plasmonic wave due to the charge transfer from 2D materials to metal film • Abundant adsorption sites for analytes and anchoring sites for various receptors via large specific surface area • Low damping effect of ultra-thin and uniform surface	• Formation of undesirable defects during transfer of 2D materials • High cost for large area and high-quality production
	Metal oxides	• Cost effective and facile synthesis for nanostructures • Catalytic effect for various chemical and bio analytes • Chemical and thermal stability	• Deterioration of SPR signals due to optical loss in visible and infrared region
	Organic composites	• Feasibility to form uniform films containing metal NPs or bioreceptors • Highly selective and sensitive detection through MIP films.	• Limitation in controlling the precise thickness at nanoscale, causing plasmon damping

DOI: 10.1039/D4TC04890C

Despite the challenges faced by LSPR and SPR sensors, ongoing research and development indicate a promising future. Advancements in nanomaterial synthesis, the incorporation of novel materials with plasmonic metals, and progress in optical technology serve as key factors for enhancing sensor performance and versatility. By functionalizing metal surfaces with organic molecules, receptors, and novel materials that selectively bind to analytes without weakening the plasmonic signals, the real-world applications of these sensors can be expanded, increasing their importance. LSPR and SPR technologies are expected to become valuable candidates in disease diagnostics, drug discovery, and environmental monitoring.

7. Conclusion

LSPR and SPR are plasmonic-based sensors that can precisely measure using optics. LSPR sensor, which detects absorbance through changes in the shape of the sensing material due to the interaction, and SPR sensor, which detects changes in refractive index that occur when the sensing material interacts with chemical adsorption, detects very low concentrations of chemicals in real time using cutting-edge sensing materials. Sensing materials for LSPR and SPR sensors exhibit important roles in improving the sensing performance of sensors, and ability of real-time detection based on rapid response. Table 3, which summarizes the general advantages and disadvantages of each sensing material, provides a clear understanding of how these materials enhance sensor performance in various applications and what roles they play. As a result, through research on sensing materials such as metal NPs, bimetal NPs, MOMs, 2D materials, metal oxides, and organic composites, have been studied, and various structures and compositions have been developed. This materials-based research enables lower detection limits and improved real-time sensing capabilities of LSPR and SPR sensors, enabling their use in a wide range of applications requiring real-time sensing, including biomedical diagnostics, environmental and industrial monitoring. In addition, LSPR and SPR sensors are able to miniaturize and can be easily measured with a light source, so they are suitable for application to portable measurement equipment, providing excellent accessibility to measurements that require real-time detection. The combined impact of sensing material improvements and practical applicability present the significant potential of LSPR and SPR sensors in driving precision and real-time sensing technologies across scientific, medical, and industrial fields, promising new answers to complex analytical challenges regarding the safe coexistence of chemicals and humanity.

Author Contributions

S. H. Cho‡, S. Choi‡, and J. M. Suh‡ contributed equally to this work.

Conflicts of interest

There are no conflicts to declare.

Data availability

Data availability is not applicable to this article as no new data were created or analysed in this study.

Acknowledgements

This work was financially supported by the Nano Material Technology Development Program (2022M3H4A1A01011993 & RS-2024-00405016) through NRF (National Research Foundation of Korea), funded by the Ministry of Science and ICT. The Inter-University Semiconductor Research Center and the Institute of Engineering Research at Seoul National University provided research facilities for this work.

References

1 T. Biswal, S. K. BadJena and D. Pradhan, *Mater Today Proc*, 2020, **30**, 274–282.

2 A. Rahimi and J. M. García, *Nat Rev Chem*, 2017, **1**, 46.

3 M. Harada, *Crit Rev Toxicol*, 1995, **25**, 1–24.

4 A. S. Ayangbenro and O. O. Babalola, *Int J Environ Res Public Health*, 2017, **14**, 94.

5 S. Lee, X. Bi, R. B. Reed, J. F. Ranville, P. Herckes and P. Westerhoff, *Environ Sci Technol*, 2014, **48**, 10291–10300.

6 W. B. Dunn, D. Broadhurst, P. Begley, E. Zelena, S. Francis-McIntyre, N. Anderson, M. Brown, J. D. Knowles, A. Halsall and J. N. Haselden, *Nat Protoc*, 2011, **6**, 1060–1083.

7 N. P. Ivleva, *Chem Rev*, 2021, **121**, 11886–11936.

8 M. Rana and V. Mittal, *IEEE Sens J*, 2020, **21**, 1187–1207.

9 Q. Pang, D. Lou, S. Li, G. Wang, B. Qiao, S. Dong, L. Ma, C. Gao and Z. Wu, *Advanced Science*, 2020, **7**, 1902673.

10 M. Javaid, A. Haleem, R. P. Singh, S. Rab and R. Suman, *Sensors International*, 2021, **2**, 100110.

11 M. Jayaweera, H. Perera, B. Gunawardana and J. Manatunge, *Environ Res*, 2020, **188**, 109819.

12 S. H. Cho, J. M. Suh, T. H. Eom, T. Kim and H. W. Jang, *Electronic Materials Letters*, 2021, **17**, 1–17.

13 S. H. Cho, M.-J. Choi, B. Koo, J. Kim, T. H. Lee, J. M. Suh, T. H. Eom, S. Y. Park, T. Kim and W. Jung, *Sens Actuators B Chem*, 2024, **403**, 135137.

14 S. Hwan Cho, J. Min Suh, B. Jeong, T. Hyung Lee, K. Soon Choi, T. Hoon Eom, T. Kim and H. Won Jang, *Chemical Engineering Journal*, 2022, **446**, 136862.

15 C. W. Lee, J. M. Suh, S. Choi, S. E. Jun, T. H. Lee, J. W. Yang, S. A. Lee, B. R. Lee, D. Yoo, S. Y. Kim, D. S. Kim and H. W. Jang, *NPJ 2D Mater Appl*, 2021, **5**, 1–13.

16 A. Kumar and R. Prajesh, *Sens Actuators A Phys*, 2022, **339**, 113498.

17 Q. Duan, Y. Liu, S. Chang, H. Chen and J. Chen, *Sensors*, 2021, **21**, 5262.

18 J. Homola, S. S. Yee and G. Gauglitz, *Sens Actuators B Chem*, 1999, **54**, 3–15.

19 J. N. Anker, W. P. Hall, O. Lyandres, N. C. Shah, J. Zhao and R. P. Van Duyne, *Nat Mater*, 2008, **7**, 442–453.

20 J. Homola, *Chem Rev*, 2008, **108**, 462–493.

21 K. M. Mayer and J. H. Hafner, *Chem Rev*, 2011, **111**, 3828–3857.

22 J.-F. Masson, *Analyst*, 2020, **145**, 3776–3800.

23 G. Simone, *Crit Rev Anal Chem*, 2024, **54**, 2183–2208.

24 J. Homola, *Anal Bioanal Chem*, 2003, **377**, 528–539.

25 X. Zhang, Z. Li, W. Yan, A. Li, F. Zhang, X. Li, M. Lu and W. Peng, *Talanta*, 2024, **269**, 125440.

26 S. Long, J. Cao, Y. Wang, S. Gao, N. Xu, J. Gao and W. Wan, *Sensors and Actuators Reports*, 2020, **2**, 100016.

27 G. Mie, *Ann Phys*, 1908, **330**, 377–445.

28 K. Matsubara, S. Kawata and S. Minami, *Appl Spectrosc*, 1988, **42**, 1375–1379.

29 K. Matsubara, S. Kawata and S. Minami, *Opt Lett*, 1990, **15**, 75–77.

30 G. Cappi, F. M. Spiga, Y. Moncada, A. Ferretti, M. Beyeler, M. Bianchessi, L. Decosterd, T. Buclin and C. Guiducci, *Anal Chem*, 2015, **87**, 5278–5285.

31 V. G. Kravets, F. Schedin, A. V Kabashin and A. N. Grigorenko, *Opt Lett*, 2010, **35**, 956–958.

32 M. Pirzada and Z. Altintas, *Micromachines (Basel)*, 2020, **11**, 356.

33 K. M. Mayer and J. H. Hafner, *Chem Rev*, 2011, **111**, 3828–3857.

34 P. Englebienne, A. Van Hoonacker and M. Verhas, *Journal of Spectroscopy*, 2003, **17**, 255–273.

35 J. Chen, A. A. Jackson, V. M. Rotello and S. R. Nugen, *Small*, 2016, **12**, 2469–2475.

36 X. Liu, J. Wang, Y. Wang, C. Huang, Z. Wang and L. Liu, *ACS Omega*, 2021, **6**, 23630–23635.

37 A. Amirjani, M. Bagheri, M. Heydari and S. Hesaraki, *Nanotechnology*, 2016, **27**, 375503.

38 J. Lerdsri, W. Chananchana, J. Upan, T. Sridara and J. Jakmunee, *Sens Actuators B Chem*, 2020, **320**, 128356.

39 Q. Zhu, T. Li, Y. Ma, Z. Wang, J. Huang, R. Liu and Y. Gu, *RSC Adv*, 2017, **7**, 19250–19256.

40 S. Rasheed, N. Ahmad, M. A. ul Haq, W. Ahmad and D. Hussain, *Journal of Industrial and Engineering Chemistry*, 2023, **128**, 450–458.

41 Z. Zhang, Z. Chen, C. Qu and L. Chen, *Langmuir*, 2014, **30**, 3625–3630.

42 P. Huang, B. Liu, W. Jin, F. Wu and Y. Wan, *Journal of Nanoparticle Research*, 2016, **18**, 1–9.

43 K. Shrivas, R. Shankar and K. Dewangan, *Sens Actuators B Chem*, 2015, **220**, 1376–1383.

44 S. Chen, J. Tang, Y. Kuang, L. Fu, F. Ma, Y. Yang, G. Chen and Y. Long, *Sens Actuators B Chem*, 2015, **221**, 1182–1187.

45 H. He, X. Xu, H. Wu and Y. Jin, *Adv Mater*, 2012, **24**, 1736–1740.

46 Y. Wang, P. Zhang, W. Fu and Y. Zhao, *Biosens Bioelectron*, 2018, **122**, 183–188.

47 Y. Wang, P. Zhang, X. Mao, W. Fu and C. Liu, *Sens Actuators B Chem*, 2016, **231**, 95–101.

48 Y. Wang, Y. Zeng, W. Fu, P. Zhang, L. Li, C. Ye, L. Yu, X. Zhu and S. Zhao, *Anal Chim Acta*, 2018, **1002**, 97–104.

49 H. Lee, H. K. Sung, C. Park and Y. Kim, *Journal of industrial and engineering chemistry*, 2017, **48**, 235–241.

50 I. Darmadi, S. Z. Khairunnisa, D. Tomecek and C. Langhammer, *ACS Appl Nano Mater*, 2021, **4**, 8716–8722.

51 X. Li, X. Lin, S. Lin, X. Sun, D. Gao, B. Liu, H. Zhao, J. Zhang, S. Cong and L. Wang, *ACS Appl Nano Mater*, 2019, **2**, 3161–3168.

52 J.-K. Chen, S.-M. Zhao, J. Zhu, J.-J. Li and J.-W. Zhao, *J Alloys Compd*, 2020, **828**, 154392.

53 Z. Qiu, Y. Xue, J. Li, Y. Zhang, X. Liang, C. Wen, H. Gong and J. Zeng, *Chinese Chemical Letters*, 2021, **32**, 2807–2811.

54 S. Li, T. Wei, M. Tang, F. Chai, F. Qu and C. Wang, *Sens Actuators B Chem*, 2018, **255**, 1471–1481.

55 Y. Xia, J. Ye, K. Tan, J. Wang and G. Yang, *Anal Chem*, 2013, **85**, 6241–6247.

56 Z. Karimzadeh, A. Jouyban, M. Khoubnasabjafari, A. Gharakhani and E. Rahimpour, *Plasmonics*, 2022, **17**, 1999–2008.

57 H.-M. Kim, W.-J. Kim, K.-O. Kim, J.-H. Park and S.-K. Lee, *J Alloys Compd*, 2021, **884**, 161140.

58 D. Sahu, N. Sarkar, G. Sahoo, P. Mohapatra and S. K. Swain, *Sens Actuators B Chem*, 2017, **246**, 96–107.

59 A. R. Ferhan, L. Guo, X. Zhou, P. Chen, S. Hong and D.-H. Kim, *Anal Chem*, 2013, **85**, 4094–4099.

60 S. S. Dandu, D. J. Joshi, T. J. Park and S. K. Kailasa, *Appl Spectrosc*, 2023, **77**, 360–370.

61 I. E. Paul, A. Rajeshwari, T. C. Prathna, A. M. Raichur, N. Chandrasekaran and A. Mukherjee, *Analytical Methods*, 2015, **7**, 1453–1462.

62 J. Song, F. Wu, Y. Wan and L. Ma, *Food Control*, 2015, **50**, 356–361.

63 I. Onyido, A. R. Norris and E. Buncel, *Chem Rev*, 2004, **104**, 5911–5930.

64 F. J. Gifford, R. M. Gifford, M. Eddleston and N. Dhaun, *Kidney Int Rep*, 2017, **2**, 282–292.

65 M. Fisser, R. A. Badcock, P. D. Teal and A. Hunze, *Sens Actuators B Chem*, 2018, **259**, 10–19.

66 S. H. Cho, J. M. Suh, B. Jeong, T. H. Lee, K. S. Choi, T. H. Eom, T. Kim and H. W. Jang, *Chemical Engineering Journal*, 2022, **446**, 136862.

67 C. Wadell, S. Syrenova and C. Langhammer, *ACS Nano*, 2014, **8**, 11925–11940.

68 L. Boon-Brett, J. Bousek, G. Black, P. Moretto, P. Castello, T. Hübert and U. Banach, *Int J Hydrogen Energy*, 2010, **35**, 373–384.

69 H. Gao, M. Liu, Z. Zhao, C. Yang, L. Zhu, Y. Cai, Y. Yang and Z. Hu, *ACS Appl Mater Interfaces*, 2020, **12**, 9693–9700.

70 S. Chang, L. Liu, C. Mu, F. Wen, J. Xiang, K. Zhai, B. Wang, L. Wu, A. Nie and Y. Shu, *J Colloid Interface Sci*, 2023, **651**, 938–947.

71 J. Feng, J. Gao, W. Yang, Y. Li, J. Shi, C. Liu, M. Jiang and S. Jiang, *ACS Appl Nano Mater*, 2023, **6**, 12775–12783.

72 P. Thawany, A. Khanna, U. K. Tiwari and A. Deep, *Sci Rep*, 2023, **13**, 5297.

73 Q. Wu, N. Li, Y. Wang, Y. Xu, S. Wei, J. Wu, G. Jia, X. Fang, F. Chen and X. Cui, *Biosens Bioelectron*, 2019, **144**, 111697.

74 Y. Wang, Z. Mao, Q. Chen, K. Koh, X. Hu and H. Chen, *Biosens Bioelectron*, 2022, **201**, 113954.

75 J. Ma, B. Lu, P. Zhang, D. Li and K. Xu, *Sens Actuators A Phys*, 2023, **353**, 114227.

76 T. Xue, W. Liang, Y. Li, Y. Sun, Y. Xiang, Y. Zhang, Z. Dai, Y. Duo, L. Wu and K. Qi, *Nat Commun*, 2019, **10**, 28.

77 S. H. Cho, J. M. Suh, W. Kim, J. Kim, Y. J. Kim, T. H. Lee, J. Y. Kim, J. Sim, S. W. Choi and B. H. Hong, *Energy & Environmental Materials*, e12801.

78 S. Gan, B. Ruan, Y. Xiang and X. Dai, *IEEE Sens J*, 2020, **21**, 347–352.

79 R. Chen, C. Guo, G. Lan, P. Luo, J. Yi and W. Wei, *Biosens Bioelectron*, 2023, 115469.

80 R. Kant, R. Tabassum and B. D. Gupta, *Biosens Bioelectron*, 2018, **99**, 637–645.

81 T. O. C. Rahayu, N. L. W. Septiani, G. Gumilar, D. R. Adhika and B. Yuliarto, *IEEE Sens J*, 2021, **21**, 19959–19966.

82 B. Karki, Y. Trabelsi, A. Pal, S. A. Taya and R. B. Yadav, *Opt Mater (Amst)*, 2024, **147**, 114555.

83 G. Kaur, A. Paliwal, M. Tomar and V. Gupta, *Biosens Bioelectron*, 2016, **78**, 106–110.

84 R. Kant, *Microchimica Acta*, 2020, **187**, 1–11.

85 A. Paliwal, A. Sharma, M. Tomar and V. Gupta, *Sens Actuators B Chem*, 2015, **216**, 497–503.

86 S. K. Mishra, S. Rani and B. D. Gupta, *Sens Actuators B Chem*, 2014, **195**, 215–222.

87 A. Paliwal, A. Sharma, M. Tomar and V. Gupta, *Sens Actuators B Chem*, 2017, **250**, 679–685.

88 Y. Mustapha Kamil, S. H. Al-Rekabi, M. H. Abu Bakar, Y. W. Fen, H. A. Mohammed, N. H. Mohamed Halip, M. T. Alresheedi and M. A. Mahdi, *Photonic Sensors*, 2022, **12**, 220306.

89 D. Zhang, Y. Sun, Q. Wu, P. Ma, H. Zhang, Y. Wang and D. Song, *Talanta*, 2016, **146**, 364–368.

90 S. Jiang, Y. Peng, B. Ning, J. Bai, Y. Liu, N. Zhang and Z. Gao, *Sens Actuators B Chem*, 2015, **221**, 15–21.

91 J. Zhang, Y. Sun, H. Zhang, B. Xu, H. Zhang and D. Song, *Anal Chim Acta*, 2013, **769**, 114–120.

92 X. Xu, Y. Zhang, B. Wang, L. Luo, Z. Xu and X. Tian, *RSC Adv*, 2018, **8**, 32538–32544.

93 S. Nangare and P. Patil, *Int J Biol Macromol*, 2022, **214**, 568–582.

94 A. Baliyan, P. Bhatia, B. D. Gupta, E. K. Sharma, A. Kumari and R. Gupta, *Sens Actuators B Chem*, 2013, **188**, 917–922.

95 A. M. Shrivastav, S. P. Usha and B. D. Gupta, *Biosens Bioelectron*, 2016, **79**, 150–157.

96 O. Çelik, Y. Saylan, I. Göktürk, F. Yılmaz and A. Denizli, *Talanta*, 2023, **253**, 123939.

97 N. Atar, T. Eren, M. L. Yola and S. Wang, *Sens Actuators B Chem*, 2015, **216**, 638–644.

98 R. Verma and B. D. Gupta, *Food Chem*, 2015, **166**, 568–575.

99 K. Chung, J. S. Lee, E. Kim, K. Lee, K. Kim, J. Lee, D. Kim, S. O. Kim, S. Jeon and H. Park, *Adv Mater Interfaces*, 2018, **5**, 1800433.

100 S. H. Choi, Y. L. Kim and K. M. Byun, *Opt. Express*, 2011, **19**, 458–466.

101 G. M. Varghese, R. John, A. Manesh, R. Karthik and O. C. Abraham, *Indian J Med Res*, 2020, **151**, 401.

102 T. Ohmi, S. Sudoh and H. Mishima, *IEEE Transactions on semiconductor manufacturing*, 1994, **7**, 440–446.

103 D. Shin, H. R. Kim and B. H. Hong, *Nanoscale Adv*, 2021, **3**, 1404–1412.

104 A. Das, S. Pisana, B. Chakraborty, S. Piscanec, S. K. Saha, U. V Waghmare, K. S. Novoselov, H. R. Krishnamurthy, A. K. Geim, A. C. Ferrari and A. K. Sood, *Nat Nanotechnol*, 2008, **3**, 210–215.

105 C. W. Lee, S. E. Jun, S. J. Kim, T. H. Lee, S. A. Lee, J. W. Yang, J. H. Cho, S. Choi, C. Kim, S. Y. Kim and H. W. Jang, *InfoMat*, 2023, **5**, e12427.

106 C. Lin and S. Chen, *Opt Commun*, 2019, **445**, 155–160.

107 A. Salinas-Castillo, I. Pastor, R. Mallavia and C. R. Mateo, *Biosens Bioelectron*, 2008, **24**, 1053–1056.

108 A. Bornø, L. Foged and G. van Hall, *Journal of mass spectrometry*, 2014, **49**, 980–988.

109 P. Kalimuthu, S. Leimkühler and P. V Bernhardt, *Anal Chem*, 2012, **84**, 10359–10365.

110 J. K. Kirk and J. Stegner, *J Diabetes Sci Technol*, 2010, **4**, 435–439.
View Article Online
DOI: 10.1039/D4TC04890C

111 R. M. Anjana, R. Pradeepa, M. Deepa, M. Datta, V. Sudha, R. Unnikrishnan, A. Bhansali, S. R. Joshi, P. P. Joshi and C. S. Yajnik, *Diabetologia*, 2011, **54**, 3022–3027.

112 R. D. Janine Freeman, C. D. E. LD and M. P. H. Lynne Lyons, *Diabetes spectrum*, 2008, **21**, 134.

113 M. Flockhart and F. J. Larsen, *Sports Medicine*, 2023, 1–9.

114 T. H. Eom, S. H. Cho, J. M. Suh, T. Kim, J. W. Yang, T. H. Lee, S. E. Jun, S. J. Kim, J. Lee, S. H. Hong and H. W. Jang, *Small*, 2022, **18**, 1–12.

115 D. Cho, J. M. Suh, S. Nam, S. Y. Park, M. Park, T. H. Lee, K. S. Choi, J. Lee, C. Ahn and H. W. Jang, *Advanced Science*, 2021, **8**, 2001883.

116 Y.-S. Shim and H. W. Jang, *Journal of Sensor Science and Technology*, 2016, **25**, 178–183.

117 G. Weinmayr, E. Romeo, M. de Sario, S. K. Weiland and F. Forastiere, *Environ Health Perspect*, 2010, **118**, 449–457.

118 Z. Xu, W. Shi, C. Yang, J. Xu, H. Liu, J. Xu and B. Zhu, *Luminescence*, 2020, **35**, 299–304.

119 T. H. Eom, S. H. Cho, J. M. Suh, T. Kim, T. H. Lee, S. E. Jun, J. W. Yang, J. Lee, S. H. Hong and H. W. Jang, *J Mater Chem A Mater*, 2021, **9**, 11168–11178.

120 C. Müller, T. Nirmaier, A. Rügemer and M. V. Schickfus, *Sens Actuators B Chem*, 2000, **68**, 69–73.

121 K. Baker, T. Rath, W. I. Lencer, E. Fiebiger and R. S. Blumberg, *Cellular and Molecular Life Sciences*, 2013, **70**, 1319–1334.

122 K. Rekha, M. D. Gouda, M. S. Thakur and N. G. Karanth, *Biosens Bioelectron*, 2000, **15**, 499–502.

View Article Online
DOI: 10.1039/D4TC04890C

123 F. Baquero, J.-L. Martínez and R. Cantón, *Curr Opin Biotechnol*, 2008, **19**, 260–265.

124 S. Ji, B. K. Min, S. K. Kim, S. Myung, M. Kang, H.-S. Shin, W. Song, J. Heo, J. Lim and K.-S. An, *Appl Surf Sci*, 2017, **419**, 252–258.

125 A. F. Coskun, A. E. Cetin, B. C. Galarreta, D. A. Alvarez, H. Altug and A. Ozcan, *Sci Rep*, 2014, **4**, 6789.

126 Y. Liu, Q. Liu, S. Chen, F. Cheng, H. Wang and W. Peng, *Sci Rep*, 2015, **5**, 12864.

127 A. G. M. da Silva, T. S. Rodrigues, J. Wang, L. K. Yamada, T. V Alves, F. R. Ornellas, R. A. Ando and P. H. C. Camargo, *Langmuir*, 2015, **31**, 10272–10278.

128 A. D. Chowdhury, F. Nasrin, R. Gangopadhyay, A. B. Ganganboina, K. Takemura, I. Kozaki, H. Honda, T. Hara, F. Abe, S. Park, T. Suzuki and E. Y. Park, *Biosens Bioelectron*, 2020, **170**, 112657.

129 S. J. Yoon and D. Kim, *J. Opt. Soc. Am. A*, 2007, **24**, 2543–2549.

View Article Online
DOI: 10.1039/D4TC04890C

View Article Online
DOI: 10.1039/D4TC04890C

Data availability

Data availability is not applicable to this article as no new data were created or analysed in this study.